



Přírodovědecká
fakulta
Faculty
of Science

Jihočeská univerzita
v Českých Budějovicích
University of South Bohemia
in České Budějovice



**JOHANNES KEPLER
UNIVERSITY LINZ**

CELLULAR PHOTOSTIMULATION WITH HYDROGEN- BONDED ORGANIC SEMICONDUCTOR MICROCRYSTAL INTERFACES



Diploma Thesis

to confer the academic degree of

Master of Science (MSc.)

in the Diploma Program

Biological Chemistry

Author

Marie Jakešová

Submission

**Linz Institute of Organic
Solar Cells (LIOS)/ Institute
of Physical Chemistry**

Thesis Supervisor

**o. Univ. Prof. Mag. Dr. DDr.
h.c. Niyazi Serdar Sariciftci**

Assistant Thesis Supervisor

**Dr. Eric Daniel Głowacki
Dr. Rainer Schindl**

November 2016

**University of South Bohemia
In České Budějovice
Faculty of Science**
Branišovská 1760
370 05 České Budějovice, CZ
www.jcu.cz

**JOHANNES KEPLER
UNIVERSITY LINZ**
Altenberger Str. 69
4040 Linz, Austria
www.jku.at
DVR 0093696

SWORN DECLARATION

I hereby declare under oath that the submitted Diploma Thesis has been written solely by me without any third-party assistance, information other than provided sources or aids have not been used and those used have been fully documented. Sources for literal, paraphrased and cited quotes have been accurately credited.

The submitted document here present is identical to the electronically submitted text document.

Ich erkläre an Eides statt, dass ich die vorliegende Masterarbeit selbstständig und ohne fremde Hilfe verfasst, andere als die angegebenen Quellen und Hilfsmittel nicht benutzt bzw. die wörtlich oder sinngemäß entnommenen Stellen als solche kenntlich gemacht habe.

Die vorliegende Masterarbeit ist mit dem elektronisch übermittelten Textdokument identisch.

Linz, 28.11.2016

Marie Jakešová

ABSTRACT

The field of (opto)electronics is one of the most developed scientific and technological disciplines. The goal of using such devices at the interface with living matter to create bioelectronic systems motivates the work in this thesis. Successful bioelectronics should rely on an active material which is biocompatible and interfaces intimately with cells. This thesis reports on biocompatible hydrogen-bonded semiconductor nanostructured crystals for cellular photostimulation. The biomimetic hierarchical crystals show impressive affinity for cellular coupling and efficient stimulation. The close interface between the nanostructured crystals and cells was elucidated using electron microscopy. Light irradiation was found to elicit a reversible electrophysiological response, measured using patch-clamp microelectrochemistry, only in cells that grow in contact with the nanostructured crystals. The mechanism of action was studied by investigating the effects of photoexcitation on specific ion channels, because it is ion pumps that cause cell depolarisation upon stimulation. In total, three different types of ion channels and two types of cells were studied. Based on the observation that the time scale of photoinduced channel activation corresponds with the time scale of photothermal heating, the heat effect was proposed as the most probable mechanism. The local rise of temperature was shown to be present upon laser irradiation of the semiconductor structures using an *in situ* electrochemical method. Other possible mechanisms could not be completely excluded, thus a more thorough research should be aimed into separation of the activation components. However, if the photothermal effect indeed predominates, the presented material would be a potent candidate for thermal cellular photostimulation, which is highly relevant to the new generation of wireless retinal implants.

ACKNOWLEDGEMENTS

I would like to thank Professor Niyazi Serdar Sariciftci for accepting and supporting me as his student and giving me the opportunity to complete my thesis at the Linz Institute of Organic Solar Cells.

My special gratitude goes to my two specialized supervisors Eric Daniel Głowacki and Rainer Schindl for their never-ending support, encouragement, guidance, fruitful discussions about science, and the fact that they were always open to new ideas. I am also grateful to Monika Litviňuková, my dear roommate who ultimately became also my valuable colleague, for all the time spent together at the patch-clamp setup. Furthermore, I would like to thank Mykhailo Sytnyk for his ideas, materials, and many hours spent together at SEM. If it was not for Eric's idea, Mykhailo's materials, Rainer's open-mindedness, Monika's time, and our critical discussions, this thesis would have never happened. Further thanks go to other LIOS colleagues for their warm acceptance, advice, and friendship, especially Dogukan Apaydin, Mateusz Bednorz, Martin Kaltenbrunner and Stepan Demchyshyn.

I would like to acknowledge the two people who made my study program of Biological Chemistry possible – Professor Libor Grubhoffer and Professor Norbert Müller. I appreciate their great support, help, and shared knowledge throughout my whole study.

Finally, I would like to thank my whole family, especially my parents, and my close friends for their encouragement, support and understanding that they have been giving me my entire life.

TABLE OF CONTENTS

1. Introduction	7
1.1. <i>Photoeffects at semiconductor/cell interface</i>	7
1.1.1. Photoconductive silicon.....	7
1.1.2. Organic semiconductors – conducting polymers	8
1.1.3. Quantum dots.....	8
1.1.4. Mechanism of cellular photo-activation	9
1.2. <i>Electrophysiology</i>	10
1.2.1. The action potential.....	10
1.2.2. The patch-clamp technique.....	11
1.2.3. RBL and HEK cells.....	12
1.3. <i>Organic pigments as semiconductors</i>	14
1.3.1. Nano-microcrystals made of organic pigments	15
2. Materials and methods	18
2.1. <i>Deposition of thin films, preparation of samples</i>	18
2.1.1. Silanisation.....	18
2.1.2. PEI-E spin-coating	18
2.1.3. Metal evaporation.....	18
2.1.4. Thin film semiconductor deposition	18
2.1.5. P3HT spin-coating.....	19
2.1.6. Carbon black substrates preparation	19
2.2. <i>Quinacridone Jeziky microstructure synthesis and deposition</i>	19
2.2.1. 513 Microstructure synthesis	19
2.2.2. 433 Microstructure synthesis	19
2.2.3. Washing procedure	19
2.3. <i>(Photo)electrochemistry, setup description</i>	20
2.4. <i>Hydrogen peroxide quantification assay</i>	21
2.5. <i>Cell culture</i>	22
2.5.1. Solutions	22
2.5.2. RBL cells	22
2.5.3. HEK cells.....	22
2.6. <i>Patch-clamp (photo)electrochemistry</i>	23
2.6.1. Solutions	23
2.6.2. The patch clamp measurement.....	24
2.7. <i>Calibrated pipette temperature measurement</i>	25
2.8. <i>Data analysis</i>	25
2.9. <i>Scanning electron microscopy (SEM)</i>	25
3. Results and discussion	26
3.1. <i>Culturing RBL cells on planar organic pigment interfaces</i>	26
3.2. <i>Culturing cells on microcrystalline QNC structures</i>	27
3.3. <i>Patch clamp results for RBL non-specific voltage-clamp</i>	29
3.4. <i>SEM investigation of QNC microstructures/cell interfaces for RBL and HEK</i>	31
3.5. <i>Patch clamp results for K⁺ inward rectifier in RBL cells</i>	34
3.5.1. Single channel analysis of K ⁺ inward rectifier in RBL cells.....	38
3.6. <i>Patch clamp results for L-type Ca²⁺ voltage-gated channels in HEK cells</i>	39

3.7. <i>Patch clamp results for temperature-gated channel TRPV1 in HEK cells</i>	42
3.8. <i>Measurement of local laser-induced heating using calibrated pipette</i>	44
3.9. <i>(Photo)electrochemistry of jeziky, hydrogen peroxide</i>	47
4. Conclusion	49
5. References	51
6. Curriculum Vitae	54

1. Introduction

Artificial neuronal stimulation is one of the topics of the new generation of medical research. Disruption of neural connections, impaired functionality or degeneration is the cause of numerous diseases and neurological problems. One of the accepted approaches to overcome these problems is the implementation of artificial electrodes. Electrostimulation is the established technology for a number of conditions such as deafness or Parkinson's disease, and is widely tested for others including Alzheimer's disease, restoration of motion, and retinal implants. These approaches are hampered by low resolution, complex wiring, limited biocompatibility of the materials and problems of achieving an intimate tissue or cell interface. An alternative to extracellular electrodes is light-induced activation. Light-directed mechanisms excel with higher resolving power and reduced wiring. A promising target for the use of light-induced stimulation of neurons is retinal prosthesis. Retinal implants are used in cases where diseases have led to the degeneration of photoreceptor cells in the retina, such as *retinitis pigmentosa* or macular degeneration. The current state-of-art in vision restoration is based on the microfabrication of electrode arrays coupled to a photosensitive material. Two mechanistic solutions have been implemented: The first relies on capture of image by an external camera, which is then transduced into an electrical signal delivered by an electrode array, which is in direct contact with the neural cells. A prominent commercial example of this is the Argus II system, made by Second Sight Medical Products Inc. The second one uses direct coupling of photodiodes to an electrodes array, e.g. "artificial silicon retina", by Optobionics corporation. The positioning of the electrode arrays can also be solved in two ways. Firstly, the implant can substitute the photoreceptors directly (subretinal) thus stimulating the bipolar cells, alternatively, it can be placed on the surface of retina (epiretinal) in order to activate retinal ganglion cells. All of the currently used implants use arrays of 60 – 5000 microelectrodes and claim to restore light sensitivity in patients, in some cases enabling them to recognize letters. However, all the technologies implemented thus far face the same problems of necessity of external powering, low resolution, invasive surgery, and questionable long-term biocompatibility of materials.^{1,2} Furthermore the electrode materials are usually not adequate for cell adhesion or growth and require additional interlayers. This problem is currently targeted with the use of conducting polymers and their composites to allow direct adhesion of cells to the electrode material and to reduce the rigidity of the inorganic electrode materials.³ An alternative approach to overcome at least some of the other drawbacks is to sensitize cells directly by electrodes with a photosensitive layer.

1.1. Photoeffects at semiconductor/cell interface

1.1.1. Photoconductive silicon

When bias is applied across a silicon wafer, a light pulse produces charge carriers at the spot of the incoming light. The local photocurrent can then activate cells in the close proximity of the light pulse. This approach was reported to photostimulate neural cells using single crystal^{4,5} or hydrogenated amorphous silicon.⁶ The stimulation can be achieved by either manipulating the voltage at constant illumination⁴ or the opposite way.⁷ Calcium imaging or patch-clamp recordings were used to verify the cellular stimulation respectively. The developed techniques showed 100 μm resolution when

using the single crystalline silicon. Amorphous silicon technology allowed thinning of the substrates and thus higher resolution, but at the price of an additional passivation layer, which again puts the studied cell in a further distance from the activation signal. The presented technologies are useful for *in vitro* studies of cell physiology, but not necessarily tractable for an artificial retina approach, since the silicon electrodes are rigid, large thickness or passivation is necessary, and the biocompatibility and stability remains unknown.

1.1.2. Organic semiconductors – conducting polymers

Soft and elastic polymer semiconductors are advantageous for cell interactions, since their material properties meet the ones of a cell better than typical inorganic semiconductors. The limiting factor in use of these materials is small efficiency of the photocurrent formation due to large exciton binding energies in organic materials. Such drawback can be overcome by using bulk heterojunction of donor and acceptor molecules. Ghezzi *et al.* used poly(3-hexylthiophene-2,5-diyl) as donor with phenyl-C61-butyric-acid-methyl ester as acceptor (P3HT/PCBM) blend to photostimulate rat embryonic hippocampal neurons. Fast neuronal activation was observed with short pulses of 532 nm laser (10 mW/mm², 20 ms) using the patch-clamp method. The authors suggest, that the heterojunction P3HT/PCBM works through a capacitive charging of the polymer-electrolyte interface, however, they did not exclude a Faradaic component. The role of ITO as substrate is claimed to be necessary for the charge separation at the interface.⁸ Later the same authors reported photo-induced stimulation of primary neuronal cells using solely P3HT on ITO as an active substrate (532 nm, 15 mW/mm², 20 ms), thus eliminating the necessity of the bulk heterojunction. This was preferred since PCBM is known to produce reactive oxygen species and thus is not optimal for biocompatibility. Further, the authors showed that such interface is capable of restoring light sensitivity in rat retinas which had been previously intentionally damaged with laser pulses.⁹ Later, another group showed induced light sensitivity in embryonic chick retinas with undeveloped photoreceptors using a blend of P3HT and a naphthalene bisimide acceptor.¹⁰ Recently the group including Ghezzi elaborated on results on the mechanism of their reported P3HT activation. They used human embryonic kidney cells as a model simpler than neurons. Their results indicate that in presence of ITO substrates a short capacitive response occurs, which is then overrun by a larger and longer thermal effect. They show that in their regime of recordings, they were increasing the local temperature by 3-7°C.¹¹ Recently, semiconducting polymer nanobioconjugate particles, engineered to interact specifically with the temperature gated transient receptor potential cation channel TRPV1, were shown to photostimulate ND7/23 neurons (880 nm, 104 μW/μm², 2s pulses).¹² The advantage of easy solution processing and lower rigidity in comparison to silicon caused large attention on conducting polymers. The advantages were though limited by the general problem of most conjugated polymers, which is their low stability in water environments.

1.1.3. Quantum dots

Semiconducting quantum dots open a wide range of possibilities for cellular interactions. Their variability in size, shape, material, surface functionalities and band gap makes them a versatile group of materials, which could allow very intimate coupling of the semiconductor and neural cell membrane, which could also be made specific.¹³ The electric dipole formed upon photoexcitation and its associated electric field should be

able to alter the membrane polarisation.¹⁴ Pappas et al. showed photocurrent-driven effects in neuroblastoma glioma cell line coming from photoreduction of oxygen using HgTe nanoparticles deposited onto an ITO substrate.¹⁵ CdTe and CdSe quantum dots were shown to activate prostatic cancer cells and cortical neurons respectively. The authors attribute the stimulation to voltage gated potassium channels. It is worth mentioning that in this study, the authors claim rather large variability between the experimental data and activation in only 10% of the cells.¹⁴ Bareket et al. reported the use of CdSe and CdS nanorods with carbon nanotubes as the interface moiety to provide larger area, roughness and biomimetic scaffold. The three dimensional matrix showed photoactivation in embryonic chick retinas with undeveloped photoreceptors.¹⁶ The key limitations of the quantum dot approach is low efficiency and limited charge transfer. Furthermore the toxicity of the nanoparticles is a major issue, since most of the materials are known to form reactive oxygen species and that the constituents of the materials such as Cd or Hg are intrinsically cytotoxic.

1.1.4. Mechanism of cellular photo-activation

Several mechanisms have been proposed for semiconductor-based interactions with cells. Three distinct mechanisms are schematically illustrated in Figure 1.

- A) Capacitive: The accumulation of photo-excited charges in the semiconductor causes the formation of an ionic layer that then perturbs the membrane polarization.¹⁷
- B) Photothermal: The photoexcited electrons, which recombine non-radiatively and thus increase the temperature of the probe and the solution in proximity of the cell. The increased temperature then causes cell depolarisation.^{18–20}
- C) Faradaic: The photoexcited electrons engage in an electrochemical reaction thereby creating redox species in the extracellular solution, which can alter the properties of the cell membrane.²¹

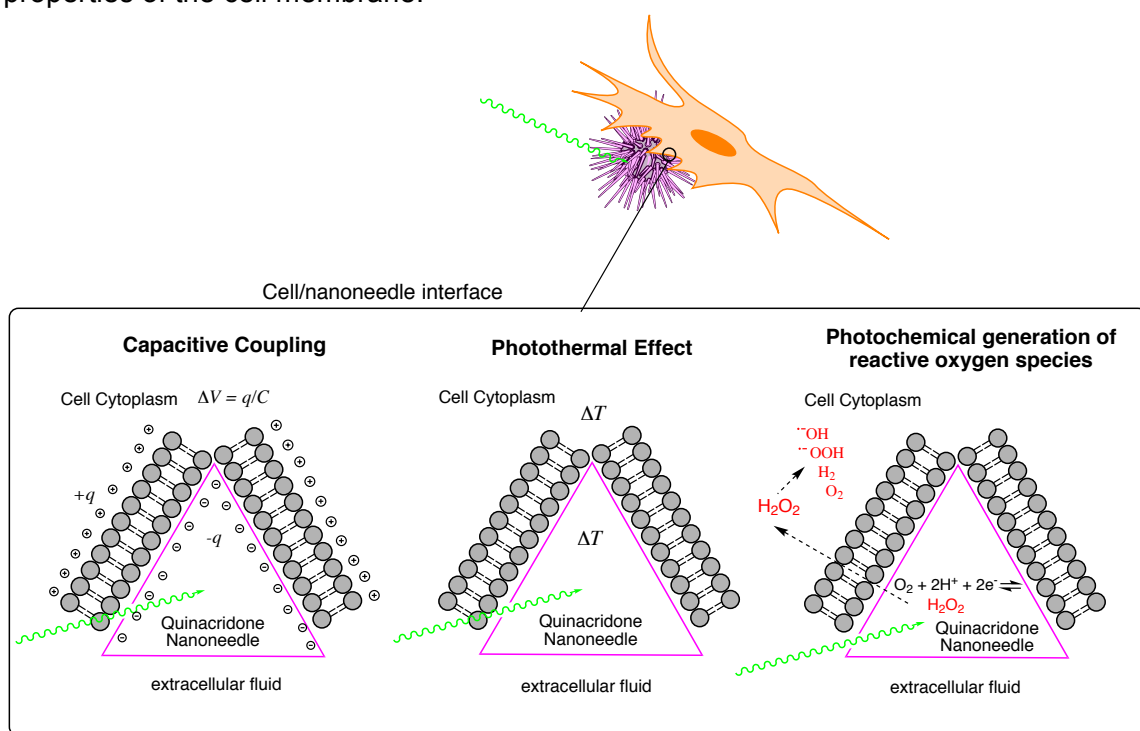


Figure 1: Schematics of the three possible mechanisms causing cell excitation upon illumination.

1.2. Electrophysiology

1.2.1. The action potential

The resting potential of a membrane is given by the different concentrations of ions inside and outside the cells. Neural cells exhibit a resting potential of typically -70 mV, which is given by the low concentration of K^+ in the extracellular liquid (4 mM out) and high concentrations of K^+ in the intracellular liquid (150 mM in). In order to transfer information, it is necessary to propagate signal from one neural cell to another. This is done partially chemically and electrically in order to provide high speed. To induce action potential, it is necessary to depolarize the membrane by approximately $+10$ mV from the resting potential of the cell. This threshold value is the “all-or-nothing” condition for the neuron to start firing. Physiologically, the whole sequence is triggered by release of neurotransmitter from the presynaptic neuron, which acts as an activator in the ligand-gated sodium channels of the postsynaptic neuron. If there is enough trigger released, the open ligand-gated ion pumps decrease the potential of the membrane to the threshold value thus causing the voltage-gated sodium channels to open and rapidly pump sodium ions inside the cell, leading to rapid further depolarisation of the cell. Once the potential becomes too positive, this activates the voltage-gated potassium channels to open and release K^+ into the extracellular space. This is necessary for the cell to return back to its resting potential. Typically the process of repolarisation overshoots, causing hyperpolarisation. This event is necessary for the neuron not to activate repeatedly without a valid trigger. The equilibrium ion concentrations are then achieved by the action of sodium-potassium ATPases.²² Further, voltage-gated sodium and potassium channels play the critical role in depolarization and repolarization, respectively. Thus by studying these specific channels under conditions of photostimulation, information about how photoeffects might eventually effect action potentials can be gained.

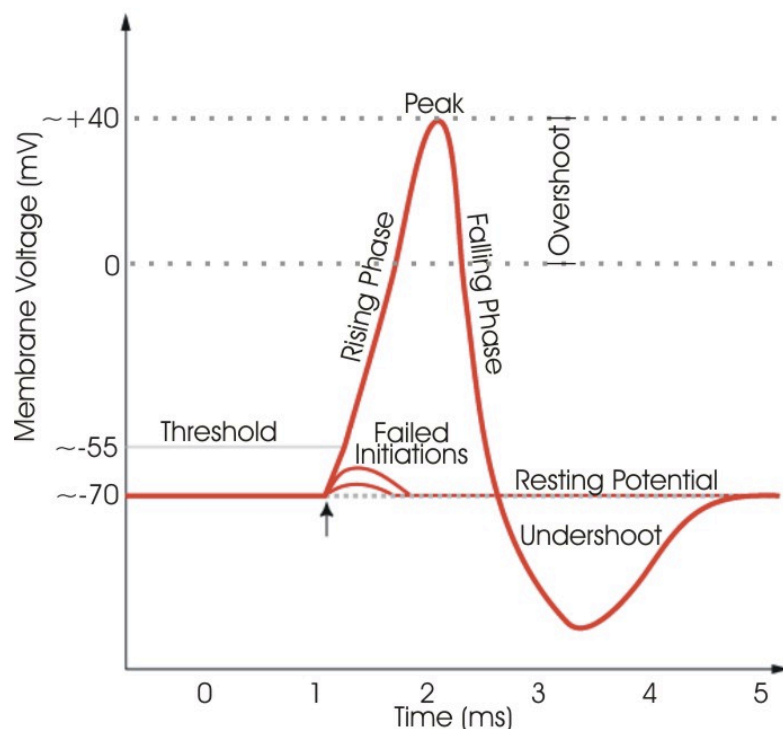


Figure 2: The action potential. Taken from Wikimedia commons.

1.2.2. The patch-clamp technique

The Noble prize winning patch-clamp technology was developed in the late 1970s by Erwin Neher and Bert Sakmann.^{23,24} This method allows the study of single and/or multiple ion channels in cells. The technique differs from the older technology of voltage clamp by applying an electrode embedded in a glass micropipette as a recording electrode and another electrode inserted in the bath solution as a reference. The micropipette has an opening on the order of a micrometre thus allowing downscaling of the membrane area to be investigated so that single channels can be analysed. The technique evolved and several variations of patch-clamp are used nowadays (Figure 3). Throughout this work, mostly whole-cell measurements were performed, in which all ion channels of the whole cell membrane are recorded at once.

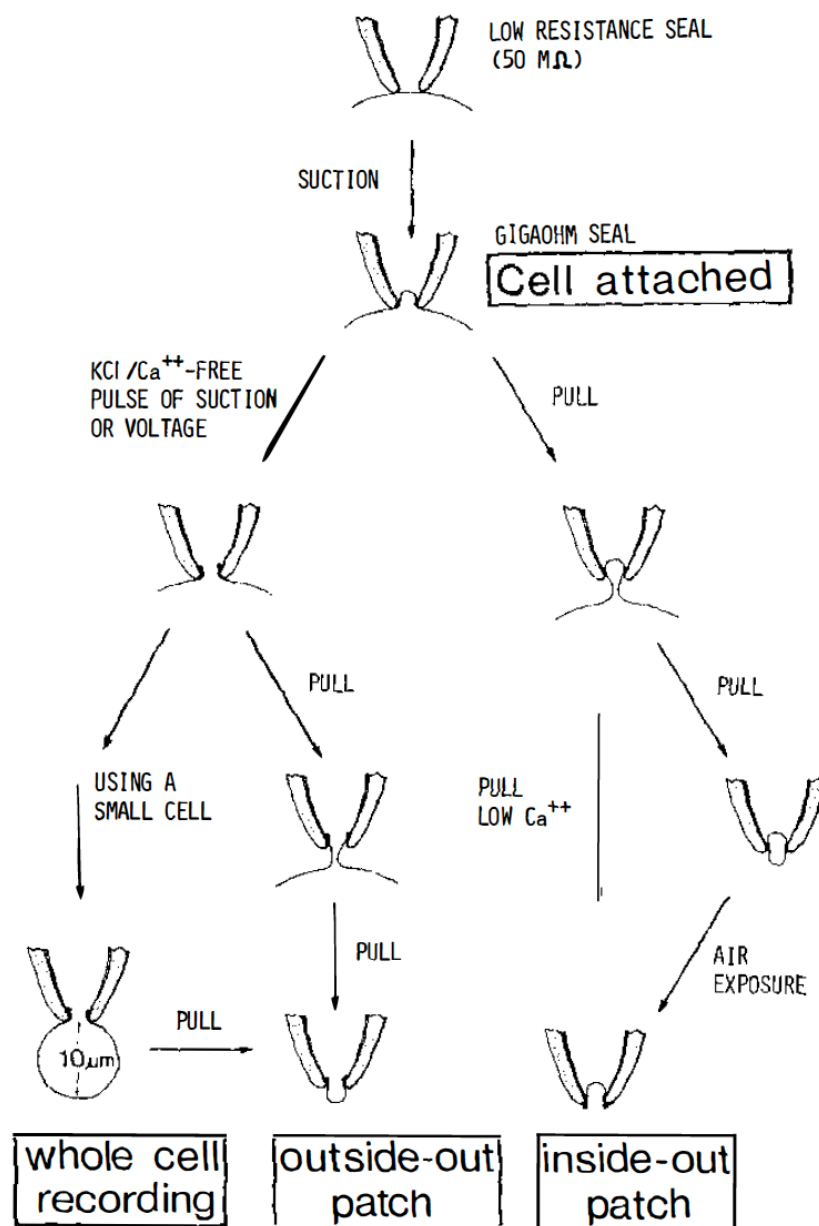


Figure 3: The configurations of patch-clamp recordings. Figure taken from [23].

The patch-clamp method is a DC technique that relies on the differential voltage clamp amplifier (Figure 4) to effectively measure small currents flowing between the patch-clamp micropipette and the bath electrode. The differential amplifier operates to make the output voltage (V_{OUT}) equal to the difference between two inputs: the desired set voltage (V_{SET}) and the input voltage (V_0). The voltage difference between set and output (i.e. micropipette) results in a current flow (i_f), which is measured over a feedback resistor. The current passed through the feedback resistor is equal to the current passing between the patch-electrode and the bath electrode, hence the trans-membrane current ($i_{membrane}$), since the latter is at ground potential.

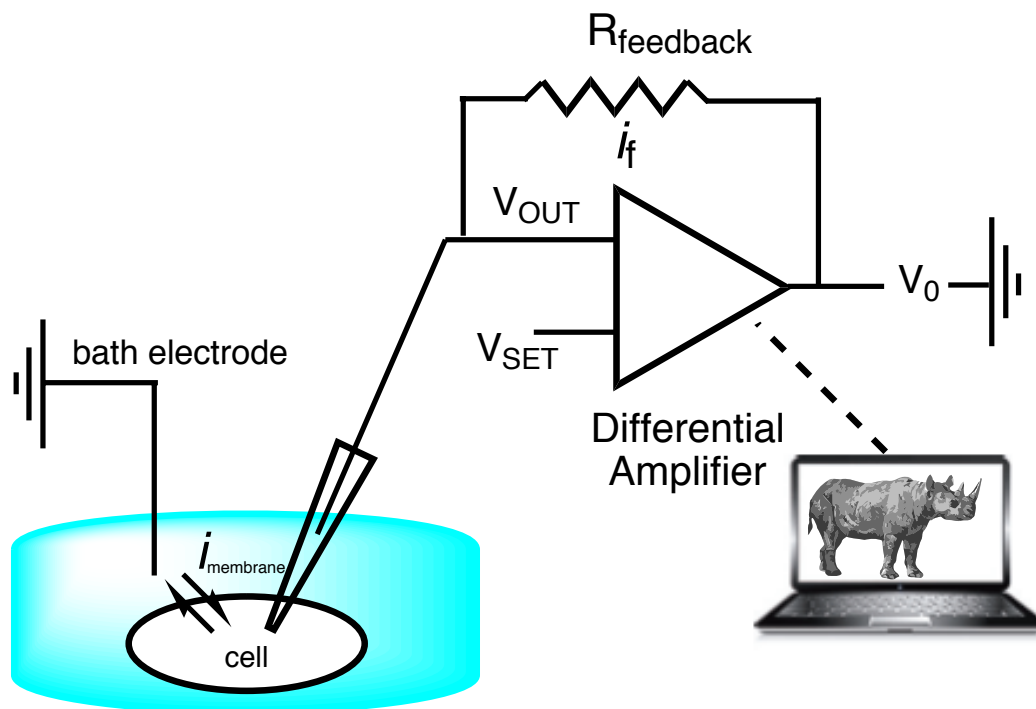


Figure 4: Schematic representation of the electrical setup of the patch-clamp technique.

The patch-clamp recording can be performed on freshly dissected cells or on cultured cells to study their native electrophysiological behaviour. Additionally, selected channels can be expressed in common cell lines allowing specific investigations. By varying the composition of the pipette and bath solutions, it is possible to study various ion channels as well as their behaviour under different conditions.

1.2.3. RBL and HEK cells

Rat basophilic leukemia cells (RBL) are histamine-secreting cells, which are responsible for inflammatory and allergic reactions in the body. The RBL-2H3 line was developed in 1978 in the Laboratory of Immunology at the National Institute of Dental Research from Wistar rat basophilic cells that were maintained as tumours. The cells grow in monolayers and are well-suited for ion channel studies.²⁵

The 293 cell line of human embryonic kidney (HEK) cells was established by transformation of HEK cells with adenovirus type 5 in 1977 by Graham et al.²⁶ The cells grow in monolayers and they exhibit rather low number of intrinsic ion channels. These

characteristics along with the relative ease of transfection made HEK293 cells one of the most common cell lines used in the study of transfected ion channels.

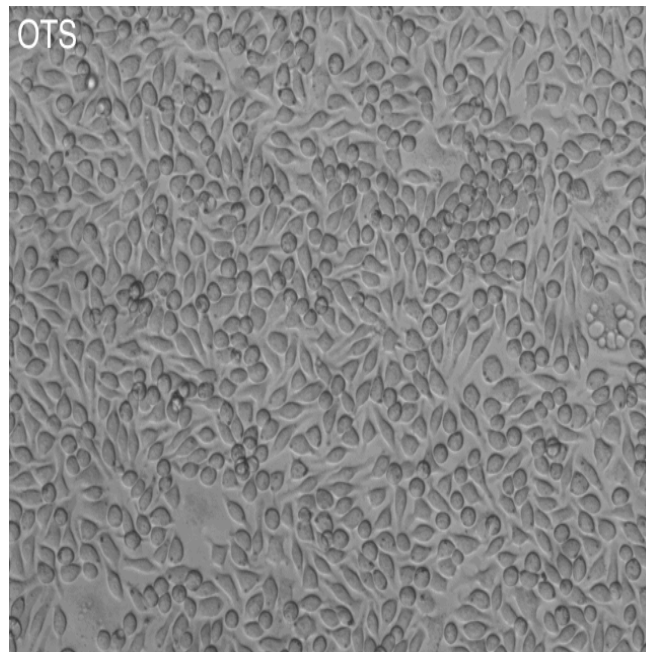


Figure 5: RBL-2H3 cells in culture on OTS-coated glass.

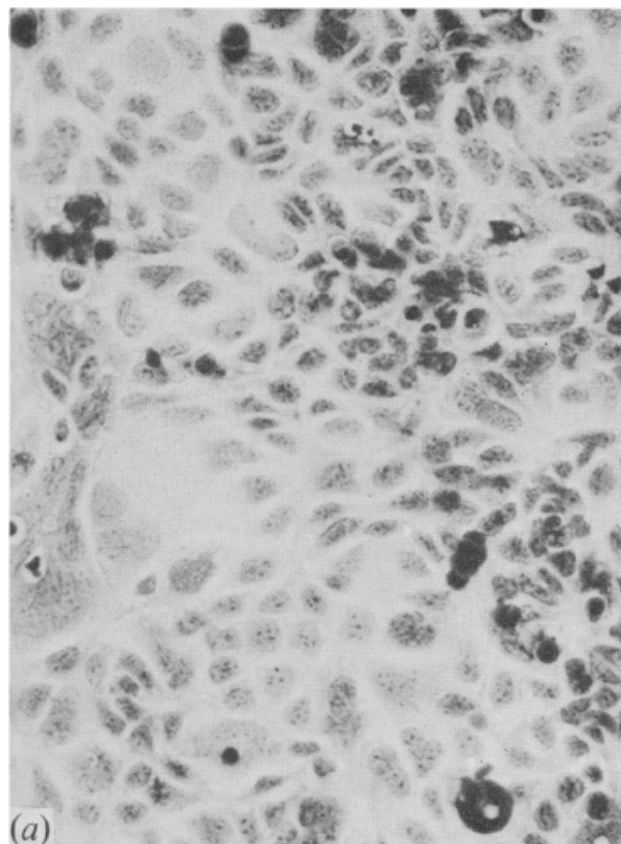
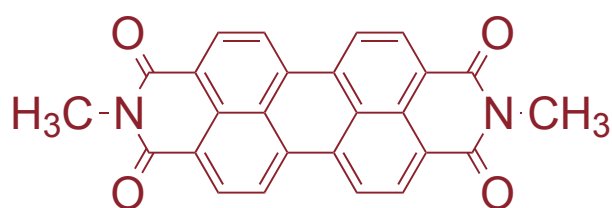


Figure 6: HEK293 cells in culture. Taken from [26]

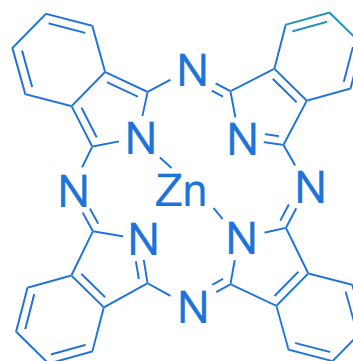
1.3. Organic pigments as semiconductors

Organic pigments are a cheap, ubiquitous group of colorants used in various industries from food, cosmetics, automotive paints, to inkjet printing. Their wide use in everyday life is motivated by their low toxicity level, low price, and high stability. A few polyaromatic conjugated pigments, such as phthalocyanines and perylene bisimides (Figure 7) were proven to be potent semiconductors.²⁷ Glowacki et al. reported in the past years, that a small molecule indigo, one of the oldest pigments used in human history, shows promising semiconducting properties when in form of thin films. This finding was highly unexpected due to the short π -conjugation within the molecule. It was, however, shown, that this molecule exhibits large intermolecular hydrogen-bonding, which helps indigo and its derivatives such as tyrian purple (Figure 7) to break the rule. The high crystalline order, the intermolecular distances and the cofacial π - π stacking play an important role in the fact that the charge can be delocalized over the molecules within a single crystal.²⁸ Strong intermolecular electronic coupling is also indicated by a large bathochromic shift when the pigment molecules in solution aggregate into the solid form. Similar behaviour was found in other small molecules such as quinacridone, the pigment in magenta printer toner, or epindolidione, the pigment in yellow toner (Figure 7). The two latter pigments showed comparatively high carrier mobilities (up to $1.5 \text{ cm}^2/\text{Vs}$) and an extraordinary stability in ambient conditions.²⁹

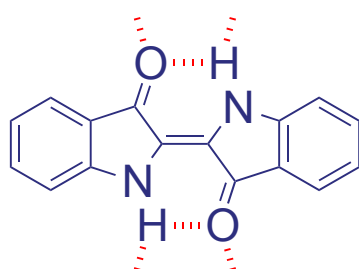
The hydrogen-bonded pigments are stable in environments not imaginable in case of other organic and inorganic semiconductors without encapsulation. The devices fabricated from hydrogen-bonded pigments are performing in ambient air, in water environment and in a wide range of pH (e.g. 3-10 for epindolidione).³⁰ In addition, it has been recently shown, that the pigments' secondary amine moieties are available for functionalization. Through a two-step reaction, it is possible to react the NH groups with a linker molecule containing a N-hydroxysuccinimide (NHS) ester on one side and the functional group of interest on the other. This can be then used to attach a molecule of choice, such as a specific antibody or an enzymatic substrate, to the surface of the semiconductor crystal.³¹ All these characteristics together make hydrogen-bonded pigments ideal candidates for use in organic electronics (low cost, air stability during operation and high carrier mobilities) as well as for the interface of organic electronics with biology (low toxicity, stability in water environment, in wide range of pH and ionic strength, possible functionalization with retained operation).



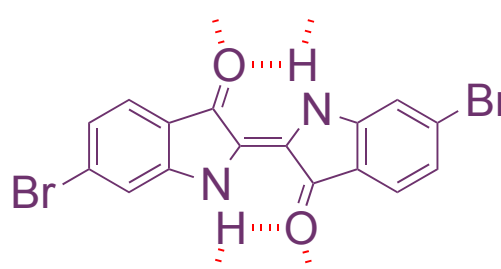
PTCDI



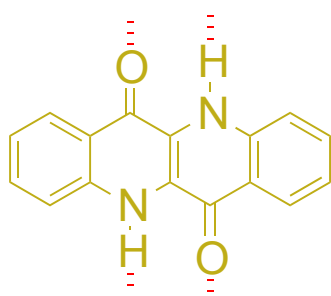
ZnPc



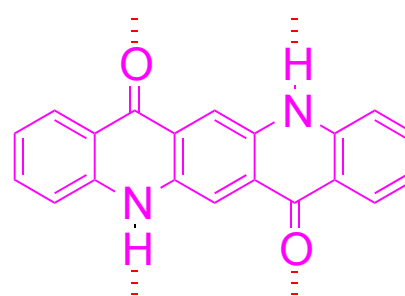
Indigo



Tyrian Purple



EPI



QNC

Figure 7: Structures of the organic pigments used in the scope of this work. Conjugated large molecules: ZnPc - zinc phthalocyanine, PTCDI = N,N'-Dimethyl-3,4,9,10-perylenedicarboximide, and hydrogen-bonded small molecules: Indigo, Tyrian Purple, EPI = epindolidione and QNC – quinacridone.

1.3.1. Nano-microcrystals made of organic pigments

Since hydrogen-bonded pigments have a very high lattice energy, vapour deposition techniques are the normal procedure for fabricating thin films. In certain biological applications, it is of an advantage to be able to solution process the materials of interest. Sytnyk et al. showed a procedure how to turn the insoluble crystalline pigments into a colloidal solution formed of single-crystal particles of various shapes and sizes. The synthesis is based on converting the materials into latent pigments by introducing a *t*-butoxycarbonyl (*t*-BOC) group onto their NH groups. This hinders the intermolecular hydrogen-bonding and thus disrupts crystallization. By controlled deprotection (heat, acid, or amine) and use of specific ligands, it is possible to hinder the growth of the

crystals in all three dimensions and thus control the shape and size. This work pioneered the field of organic micro/nanoparticles. One of the biggest advantages of these materials is that even in their form they keep the photoelectric properties in aqueous environment superior compared to their inorganic relatives such as CdSe/ZnS core/shell nanoparticles.³²



Figure 8: The synthetic route to produce colloidal solutions from pigment crystals on the example of quinacridone. (Taken from³²)

In the follow-up study concentrated on alkylamine driven deprotection of t-BOC quinacridone it was shown that it is possible to produce various 3-D (biomimetic) hierarchical microstructures by variation of the amine ligand, additives, reaction time and temperature. A further advantage of the amine deprotection route is the possibility to use ligands, which are heat or acid sensitive, since the reaction can be performed at room temperature (*under revision* Sytnyk, Jakešová et al.) This provides the possibility of production of functionalized/specific microcrystals useful in biochemical/medical engineering. Of a special interest for this study were hedgehog-like structures henceforth referred to as “jeziky” after the Pan-Slavic expression for hedgehog (Figure 9). Due to their round shape, high surface area, and pointy nanoscale spines ideal for maximizing contact area with cells, they were chosen to be used for the cell interaction/stimulation studies.

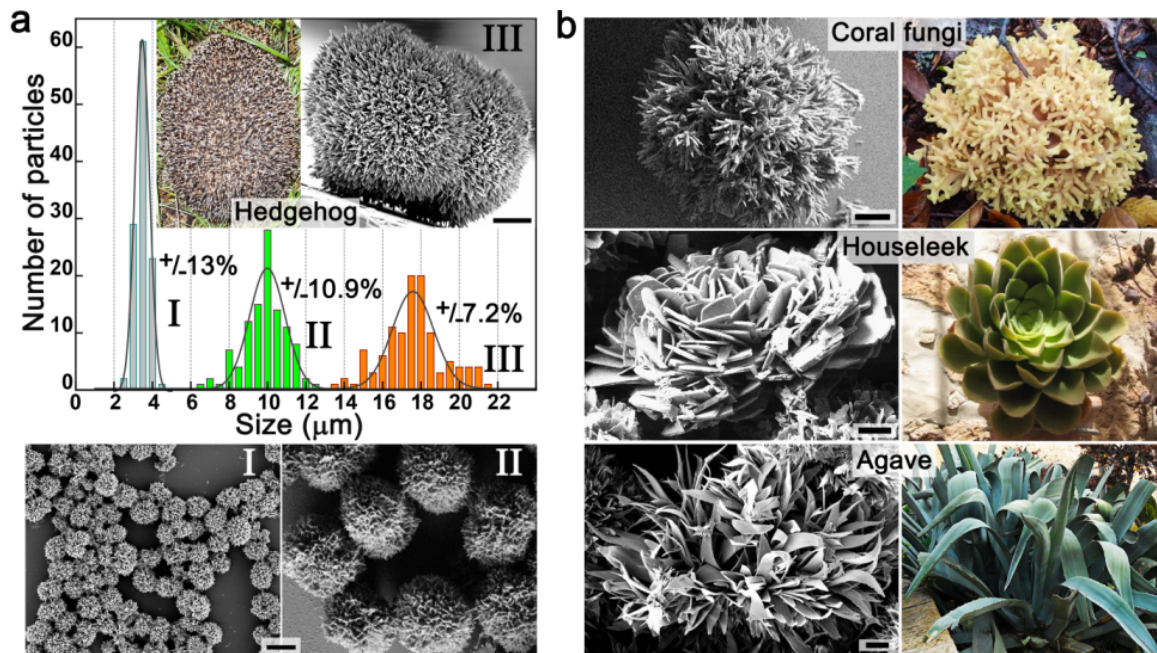


Figure 9: Biomimetic quinacridone microstructures. A) “jeziky” shaped crystals with controlled size in three narrow ranges; B) other bio-inspired shapes; all scale bars 4 μm . Taken from (under revision Sytnyk, Jakešová et al.)

2. Materials and methods

2.1. Deposition of thin films, preparation of samples

Glass substrates for electrochemistry (25.4 × 9 mm) and patch clamp (Ø12-mm) were washed by sonication in the series of acetone (RT), isopropanol (50°C), 2% hellmanex (70°C) and deionized water (RT) each for 15 minutes. The glass slides were then rinsed with 18 MΩ water, dried under a stream of N₂ and treated in oxygen plasma (50 W, 5 min) in order to remove any residual organic contaminants and to obtain a hydrophilic reactive surface.

2.1.1. Silanisation

To prepare a hydrophobic surface for the growth of thin films/attachment of crystalline microstructures the clean substrates were treated with n-octyltrichlorosilane (OTS, Alfa-Aesar) vapour (90°C overnight) in a closed glass Petri dish. In order to remove multilayer/ physisorbed OTS molecules, the slides were then rinsed with isopropanol, sonicated in toluene, rinsed with toluene, isopropanol, 18 MΩ water and dried with N₂.

2.1.2. PEI-E spin-coating

Since HEK cells prefer more hydrophilic surfaces for attachment, a different coating was necessary for experiments including this cell line. The clean substrates were spin-coated with a mixture of 2% polyethyleneimine 80% ethoxylated solution (PEI-E, Sigma Aldrich) and 2% glycerol diglycidyl ether (Sigma Aldrich) in isopropanol. The spin-coater setting was:

1. 84 rotations per second (rps), 2 s ramp, 45 s
2. 33 rps 2 s ramp, 4 s

The films were then heated to 115°C for 5 min to induce crosslinking.

2.1.3. Metal evaporation

The metal layer was prepared by physical vapour deposition of Cr, Au and Al. The metal evaporation system was operated in high vacuum (10⁻⁶ mbar), the source heating was done by leading DC current through a tungsten boat in case of Au and Al or a chromium coated tungsten rod in case of Cr. The typical rates of deposition were 0.01-0.05 nm/s for Cr, 0.5-2 nm/s for Au and 0.1-2 nm/s for Al. The thickness of the films was controlled by quartz crystal microbalance (QCM). Thickness calibration was performed using a profilometer DektakXT (Bruker). For electrochemistry purposes the film was composed of 3 nm sticking layer of Cr and 80 nm Au, a dumbbell-pattern shadow mask was used during the evaporation to pattern the metal layer. In case of patch-clamp substrates, the film consisted of 1 nm Cr and 9 nm Au to preserve transparency. The substrates were then treated with OTS vapour as indicated above. In case of metalizing the semiconductor structures on top, the thickness was 1 nm Cr and 9 nm Au or 10 nm Au or 10 nm Al.

2.1.4. Thin film semiconductor deposition

Thin films of small organic molecules were deposited onto OTS glass slides or Cr/Au/OTS substrates in a four-source PVD HANDY/40 thin film deposition system (Vaksis) allowing co-deposition of materials. The base pressure of the system was 10⁻⁷ Torr, the sources were heated by leading DC current through a tungsten coil around alumina crucibles, the thickness was monitored by QCM. Typical rates of deposition

were 0.3-0.9 Å/s for zinc phthalocyanine (ZnPc), *N,N'*-Dimethyl-3,4,9,10-perylenedicarboximide (Me₂PTCDI, BASF) and indigo (BASF); and 2-7 Å/s in case of quinacridone (Kremer Pigmente) and epindolidione (supplied by G. Romanazzi of the Polytechnic University of Bari, Italy). Tyrian purple (synthesized according to Voss and Gerlach³³) was evaporated from a hot-wall epitaxy source at a pressure of 1×10^{-7} mbar at a rate of 0.15 Å/s.

2.1.5. P3HT spin-coating

Poly(3-hexylthiophene), P3HT (Solamer), was used for comparative purposes. A 1.5 weight% solution of regioregular fractionated sample (MW > 100,000) in chlorobenzene was prepared and spin-casted:

1. 25 rps 2 s ramp, 2 s
2. 67 rps 2 s ramp, 20 s

The films were then annealed at 140°C for 10 min.

The films had a thickness of approximately 80 nm.

2.1.6. Carbon black substrates preparation

The samples for temperature control experiments were prepared by spraying carbon black spray (Graphit 33, KONTAKT CHEMIE) onto OTS treated substrates or onto clean cover slides, which were then treated with oxygen plasma (various power for 5 min) and with OTS vapour as described above. Such samples were only rinsed with 18 MΩ water after the OTS treatment.

2.2. Quinacridone Jeziky microstructure synthesis and deposition

The ready to use materials and synthetic procedures for the most potent materials were obtained from Dr. Mykhailo Sytnyk of Friedrich-Alexander-Universität Erlangen-Nürnberg, Germany. Two synthetic recipes were elaborated, known by lab protocol numbers 433 and 513, and syntheses conducted in Linz as part of this work.

2.2.1. 513 Microstructure synthesis

1.2 mL of 33 mg/mL bis-boc-quinacridone (bis-boc-Q, synthesized according to [32] by M. Sytnyk) in chloroform were injected into a stirred mixture of 2 g of dibenzoylmethane (Sigma Aldrich) dissolved in 10 mL butylamine (Alfa Aesar). After a few seconds, the stirrer was removed and the mixture was left undisturbed in dark for 24 hours to allow crystallization.

2.2.2. 433 Microstructure synthesis

Bis-boc-Q crystals were finely ground. 18 mg of the fine powder were mixed with 12 mL of oleylamine (purified, supplied by M. Sytnyk). The mixture was thoroughly shaken for 3 minutes and then was left undisturbed in dark for 24 hours to allow crystallization.

2.2.3. Washing procedure

The supernatant was removed from the crystallized products and the rest was diluted 50:50 with cyclohexane and lightly mixed. The particles were allowed to settle down. The supernatant was carefully removed, 4 mL of chloroform were added and the mixture was shaken. The colloid was again diluted with cyclohexane and the whole washing

procedure was repeated 3 times. Finally the microstructures were resuspended in 4 mL of chloroform.

The jazyky microstructures were deposited from chloroform onto Cr/Au/OTS, OTS or PEI-E coated substrates. In some cases metal layer was evaporated on top of the microstructures. In such circumstances a total of 10 nm layer was deposited and was composed of either of 10 nm Au, 1 nm Cr/ 9 nm Au or 10 nm Al.

2.3. (Photo)electrochemistry, setup description

The photoelectrochemistry measurements were done using a three-electrode setup and a potentiostat, where the working electrode was semiconductor/microstructure-modified Cr/Au, coiled platinum wire acted as a counter electrode and Ag/AgCl as a quasi-reference electrode. The whole setup was downscaled in size, by applying a polydimethylsiloxane (PDMS) block on top of the working electrode active area thus patterning each sample into a few (2-4) separate measurement cells. The total volume of the electrochemical cell was $\sim 20 \mu\text{L}$. Photocurrent was tested by applying a halogen lamp with an intensity of 50 mW/cm^2 , which was equipped with an IR filter. The electrolytes used throughout were prepared by mixing HCl (or NaOH for $\text{pH} > 7$) with addition of Na_2SO_4 in order to keep the ionic strength constant at 0.1 M. The active area (coverage with quinacridone microcrystals) of each electrode was determined individually under the microscope.

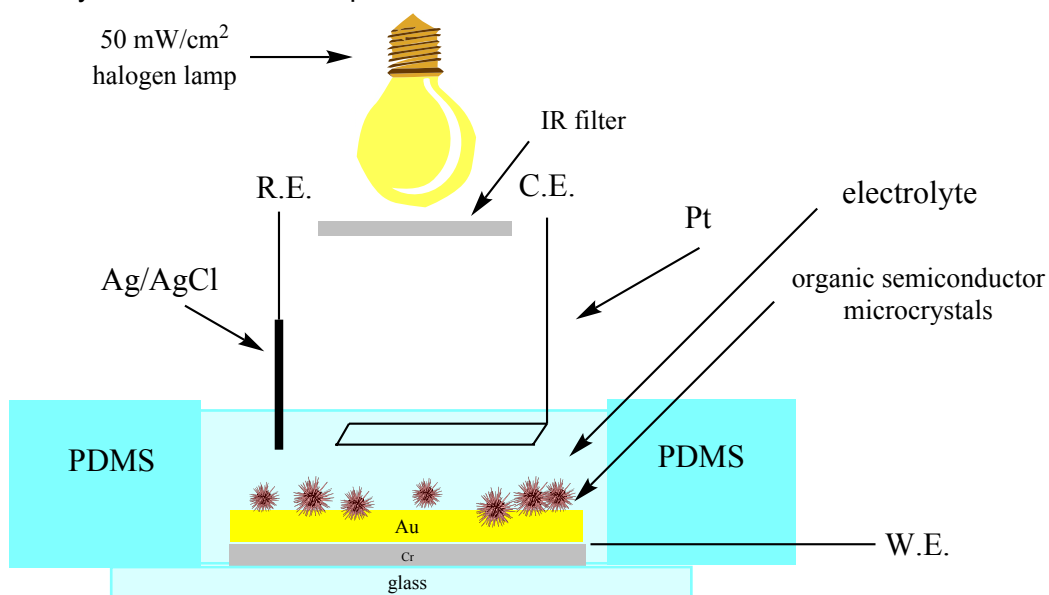


Figure 10: Electrochemistry setup with quinacridone microcrystal structures.

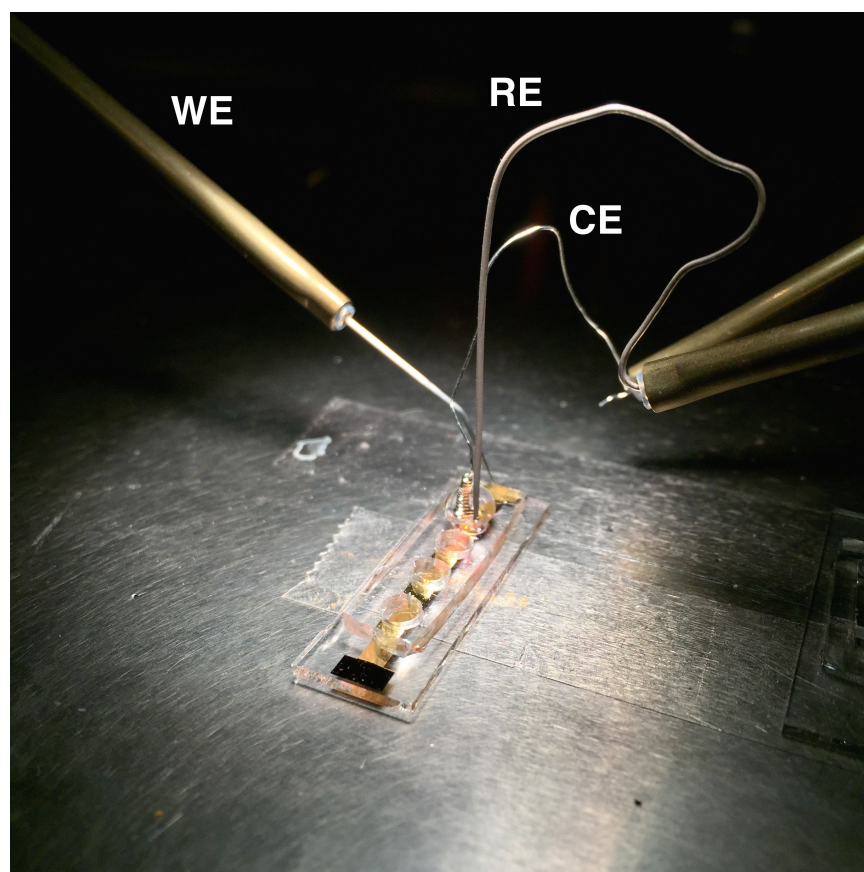


Figure 11: A photograph of the micro-electrochemistry setup, working electrode (WE) – jeziky coated Cr/Au, reference electrode (RE) – Ag/AgCl, counter electrode (CE) - Pt.

2.4. Hydrogen peroxide quantification assay

A system of horseradish peroxidase (HRP) and 3,3',5,5'-Tetramethylbenzidine (TMB) was used for H_2O_2 quantification: The amount of the produced hydrogen peroxide was tracked spectrophotometrically by following the oxidation of TMB at 653 nm using Perkin Elmer UV/VIS/NIR Spectrometer Lambda 1050.³⁴ An OTS glass slide with deposited quinacridone microstructures equipped with a PDMS barrier was filled with 150 μL of electrolyte solution and illuminated with a halogen lamp with an intensity of 50 mW/cm^2 , which was equipped with an IR filter. The electrolyte solution was added into a mixture of 0.4 $\mu\text{g}/\text{mL}$ HRP (Sigma-Aldrich) in 0.08 M citrate-phosphate buffer pH 6.0. The time measurement was started and 17 $\mu\text{g}/\text{mL}$ TMB (Sigma-Aldrich) was added giving a total of 3 mL in the cuvette. Quantification of the produced H_2O_2 was determined by the end point method using the extinction coefficient of the TMB oxidation product at 653 nm, $\epsilon = 39000 \text{ M}^{-1}\text{cm}^{-1}$.

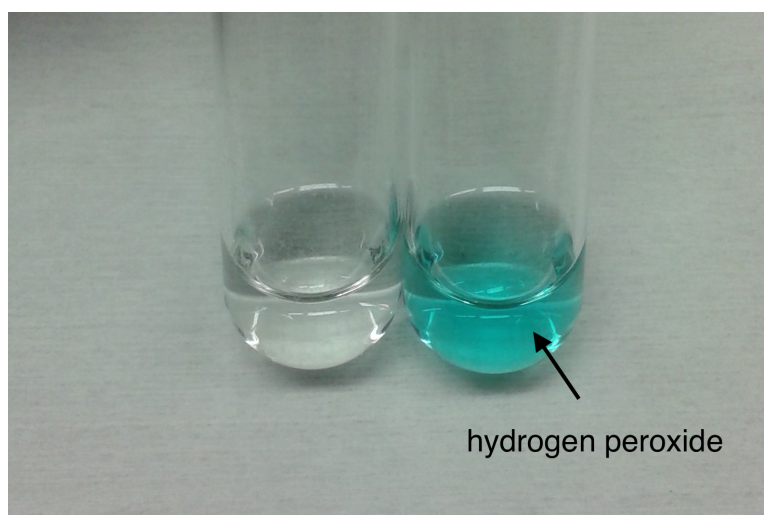


Figure 12: HRP/TMB assay in absence/presence of H₂O₂.

2.5. Cell culture

Most of the cell seeding and transfections were performed by Monika Litviňuková from the Institute of Biophysics.

2.5.1. Solutions

Dulbecco's Modified Eagle's Medium (DMEM), high glucose with sodium pyruvate, and L-glutamine (P04-05550)

MEM Eagle Minimum Essential Medium with Earle's Balanced Salt Solution (EBSS) and L-glutamine (P04-08500)

Supplements: Fetal Calf Serum (FCS) (Gibco Invitrogen #16000-044)

Penicilin/ Strep. (PAA #P11-010)

Trypsin EDTA without Ca and Mg (P10-023100)

Dulbecco's phosphate-buffered saline (DPBS) without Ca and Mg solution (P04-36500)

TransFectin™ Lipid Reagent (BioRad #170-3352)

The handling of cell culture was performed in a laminar hood in order to prevent contamination. The preparations were cultured in MEM (RBL cells) or DMEM (HEK cells) medium in an incubator (37°C, 95% humidity, 5% CO₂).

2.5.2. RBL cells

RBL cells were washed with DPBS and treated with trypsin-EDTA at 37°C for 8 minutes in order to detach them. To stop the reaction, MEM medium was then added and the cells were centrifuged. The supernatant was removed and the precipitate was resuspended in fresh MEM medium and diluted to the appropriate cell density. The cells were applied onto the experimental substrates, which were first sterilized by consecutive wash in ethanol and water 3 times. It should be mentioned that all the pigment layers used in this study were compatible with this treatment. The samples were then cultured overnight.

2.5.3. HEK cells

Since the HEK cells have a low number of intrinsic ion channels, a specific protein had to be transfected according to the type of channel intended for study. The transfection of HEK293 cells was done by the lipofection technique using TransFectin™ and 1-1.5 μg

of the target DNA. Constructs with attached yellow fluorescent protein were used, where YFP acted as a marker of positive transfection. The medium was changed after 3.5 hours post-transfection. The experiments were performed within 24-34 hours post-transfection. In the morning the cells were reseeded onto the experimental substrates using DMEM medium and the same technique as stated for RBL cells above. The slides used for HEK cells were treated with PEI-E in order to allow better attachment of the cells, since they prefer hydrophilic surfaces. The cells were measured 4 hours after reseeding.

2.6. Patch-clamp (photo)electrochemistry

All the patch-clamp experiments were done in cooperation with Monika Litviňuková or Rainer Schindl from the Institute of Biophysics, since the setup required simultaneous operation by two people for each measurement.

2.6.1. Solutions

extracellular 2 mM Ca^{2+} solution: NaCl 145 mM, KCl 5 mM, MgCl_2 1 mM, HEPES 10 mM, Glucose 10 mM, CaCl_2 2 mM, adjusted pH = 7.4 (with NaOH)

extracellular 0.3 mM Ca^{2+} solution: NaCl 145 mM, KCl 5 mM, MgCl_2 1 mM, HEPES 10 mM, Glucose 0.3 mM, CaCl_2 0.3 mM, adjusted pH = 7.4 (with CsOH)

extracellular 0 mM Ca^{2+} solution: NaCl 145 mM, KCl 5 mM, MgCl_2 1 mM, HEPES 10 mM, Glucose 10 mM, CaCl_2 0 mM, adjusted pH = 7.4 (with NaOH)

intracellular solution: Cesium methane sulfonate 145 mM, NaCl 8 mM, MgCl_2 5 mM, HEPES 10 mM, EGTA 20 mM, adjusted pH = 7.2 (with CsOH)

K^+ intracellular solution: KCl 145 mM, MgCl_2 1 mM, HEPES 10 mM, Glucose 10 mM, adjusted pH = 7.4 (with KOH)

The solutions were sterilized weekly using a 0.15 μm syringe filter.

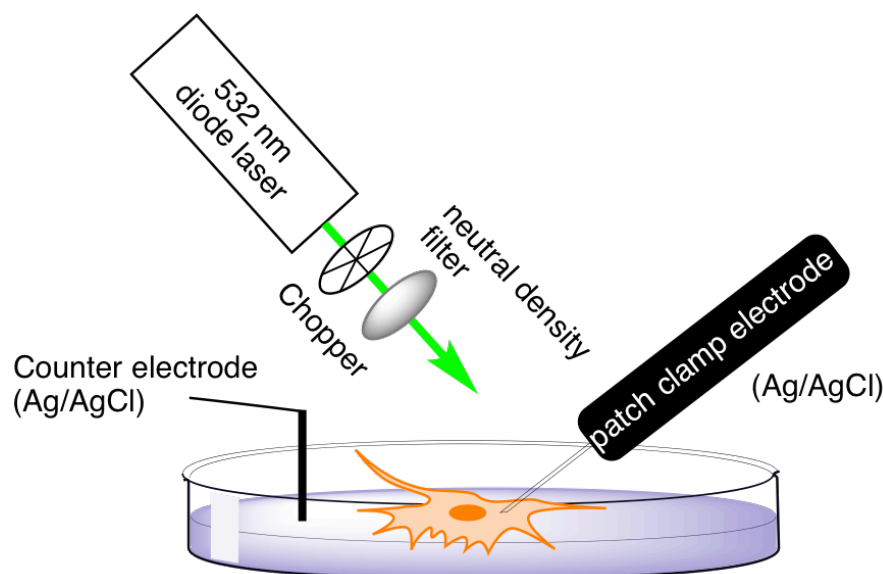


Figure F13: The patch-clamp setup.

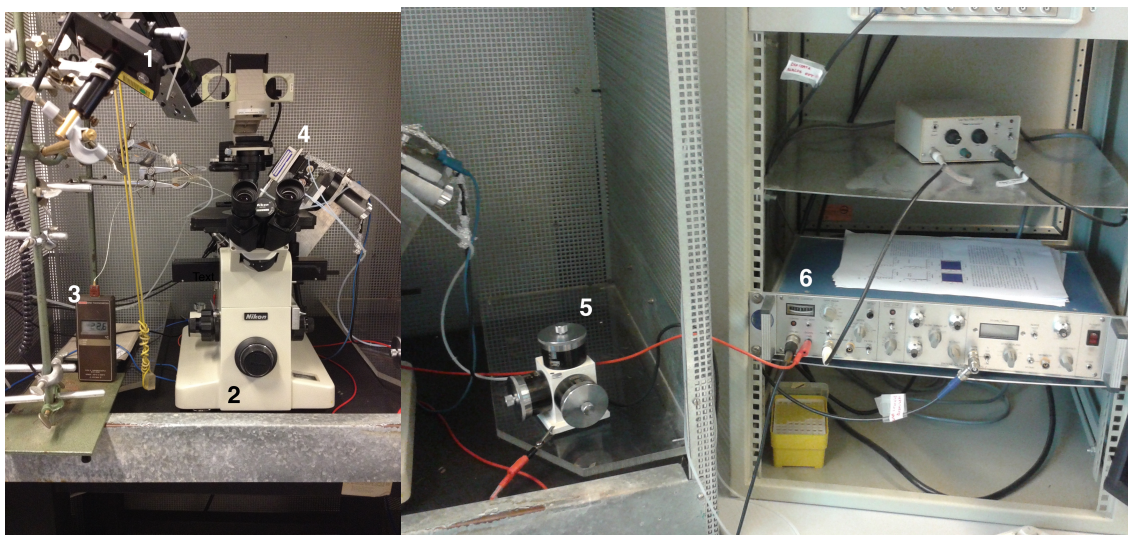


Figure 14: A photograph of the patch-clamp setup. (1) 532 nm diode laser, (2) inverted fluorescence microscope, (3) thermocouple, (4) patch-pipette holder, (5) micromanipulator, (6) amplifier

2.6.2. The patch clamp measurement

The substrates with cells were washed after culture with the 0 mM Ca^{2+} extracellular solution. The slides were applied into the sample holder, which was then filled with the 0.3 mM Ca^{2+} extracellular solution or with 2 mM Ca^{2+} extracellular solution in case of potassium channel recordings. The Ag/AgCl reference electrode was put in contact with the bath solution. Micropipettes from borosilicate glass with a typical resistance $\sim 2 \text{ k}\Omega$ were prepared using the micropipette puller. These were then filled with the intracellular solution and equipped with another Ag/AgCl electrode. An experimental/control single cell was chosen based on visible contact of the cell with the semiconductor microcrystal. In case of transfected HEK cells, sufficient fluorescence of the cell indicating successful transfection was a further selection criterion. The pipette was brought to close proximity of the cell by means of a micromanipulator. Contact between the micropipette and the cell membrane was established by mild suction thus forming a $\text{G}\Omega$ resistance. For whole-cell recordings, further suction was applied until the membrane broke. The activity of the cells was first tested in ambient conditions (23°C , room light) and then under diode laser illumination (532 nm, $\sim 4 \text{ mW}/\text{mm}^2$ when OD 0.3 applied, measured with a calibrated Hamamatsu Si diode), which was aimed at the pipette tip. Whole-cell recording configuration was performed in the following cases:

- RBL, non-selective recordings

The membrane potential was held at constant value between -40 and $+40 \text{ mV}$.

- RBL, K^+ inward rectifier

Voltage ramps between -120 mV and $+60 \text{ mV}$ lasting for 100 ms were applied from a holding potential of 0 mV .

- HEK, L-type Ca^{2+} voltage-gated channels

Constant voltage recordings were performed between -50 mV and 100 mV in 10 mV steps each lasting for 300 ms. Full range was first recorded at ambient light conditions and then with laser illumination.

- HEK, Ca^{2+} temperature dependent channel TRPV1

Voltage ramps between -100 mV and $+100 \text{ mV}$ lasting for 200 ms were applied from a holding potential of 0 mV .

Single channel activity in the cell-attached mode was recorded for K^+ inward rectifier in RBL cells. The cells were held at 0 mV, hence a voltage difference of ~ 70 mV occurred in respect to the resting potential.

2.7. Calibrated pipette temperature measurement

Glass substrate was inserted into the sample holder, which was then filled with 200 mM NaCl electrolyte solution. An Ag/AgCl electrode and a thermocouple were inserted into the bath solution. A pipette of typical resistance ~ 8 k Ω equipped with Ag/AgCl electrode and filled with the same solution as the bath, was brought in a close proximity of the thermocouple. The current was measured at constant applied voltage of 1 mV. The calibration was carried out by inserting a warm NaCl solution and recording the current as well as the temperature, which was read out from the thermocouple.

The experimental substrates were treated the same way, however, the probed spot was chosen in a way that the microcrystalline structure was in such a distance from the pipette tip as if a cell was in between. The laser beam was aimed at the end of the pipette. The local temperature was calculated from the calibration curve.

2.8. Data analysis

The analysis of the patch clamp data was done using the software WinWCP, Strathclyde Electrophysiology Software. Further analysis and evaluation was performed in Origin, OriginLab Software.

2.9. Scanning electron microscopy (SEM)

The samples for SEM were consisting of OTS or PEI-E covered glass slides with deposited quinacridone microstructures. Such substrates were then seeded with RBL or HEK cell culture. After the appropriate cultivation time, the cells were fixed in 2% glutaraldehyde solution in PBS with added 200 mM glucose (PBS-G) for 1 hour at RT. They were then washed with PBS-G three times and kept in fresh PBS-G at 4°C. The samples were then dehydrated using solutions of increasing percentage of ethanol in water. The sequence was the following: 50%, 60%, 70%, 80%, 90%, 95% (2 \times) and fresh 100% (3 \times); each step was performed for 15 min, the last step for 10 min each. Finally, a ~ 30 nm Au film was evaporated on top of the dry samples as described in 2.2. The samples were then measured using scanning electron microscope Zeiss XB 1540. The acceleration voltage was set to 5 kV. Imaging was accomplished using the in-lens detector, or a secondary-electron detector for better topological resolution.

3. Results and discussion

3.1. Culturing RBL cells on planar organic pigment interfaces

As the first step in this study, the compatibility of the hydrogen-bonded pigment semiconductor materials with the RBL cell line was performed with regard to the necessity of the cells to attach to the studied surface. For executing of a patch-clamp experiment, the cells have to be immobilised. The cell culture was grown on glass slides treated with OTS, which were patterned with areas of evaporated thin films of the experimental materials (Figure 15). In all cases the cells exhibited no difference in growth on the OTS glass and on the pigments (Figure 16). Furthermore all the pigments showed to be robust in the water environment of the culture medium.

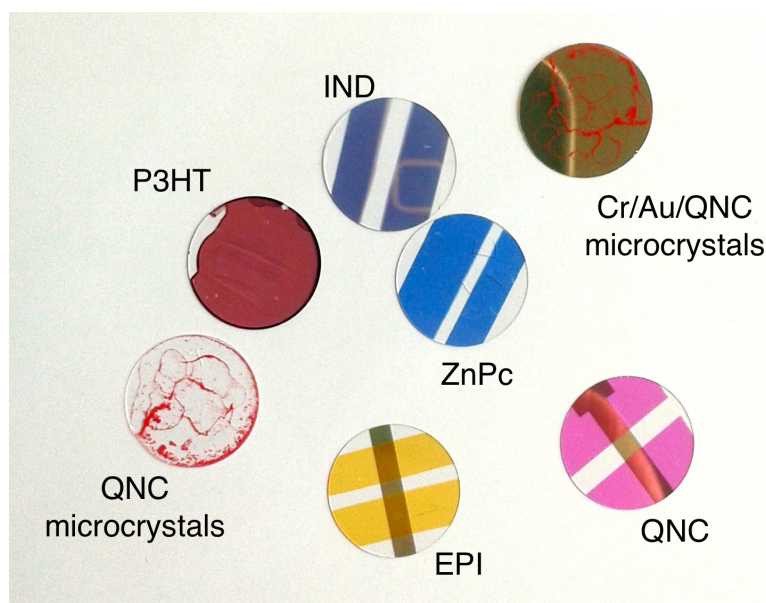


Figure 15: Examples of the experimental glass slides. EPI – Epindolidione (with Cr/Au stripe), IND - Indigo, P3HT – poly(3-hexylthiophene), QNC – Quinacridone (with Cr/Au stripe), ZnPc - Zinc Phthalocyanine and QNC microstructures.

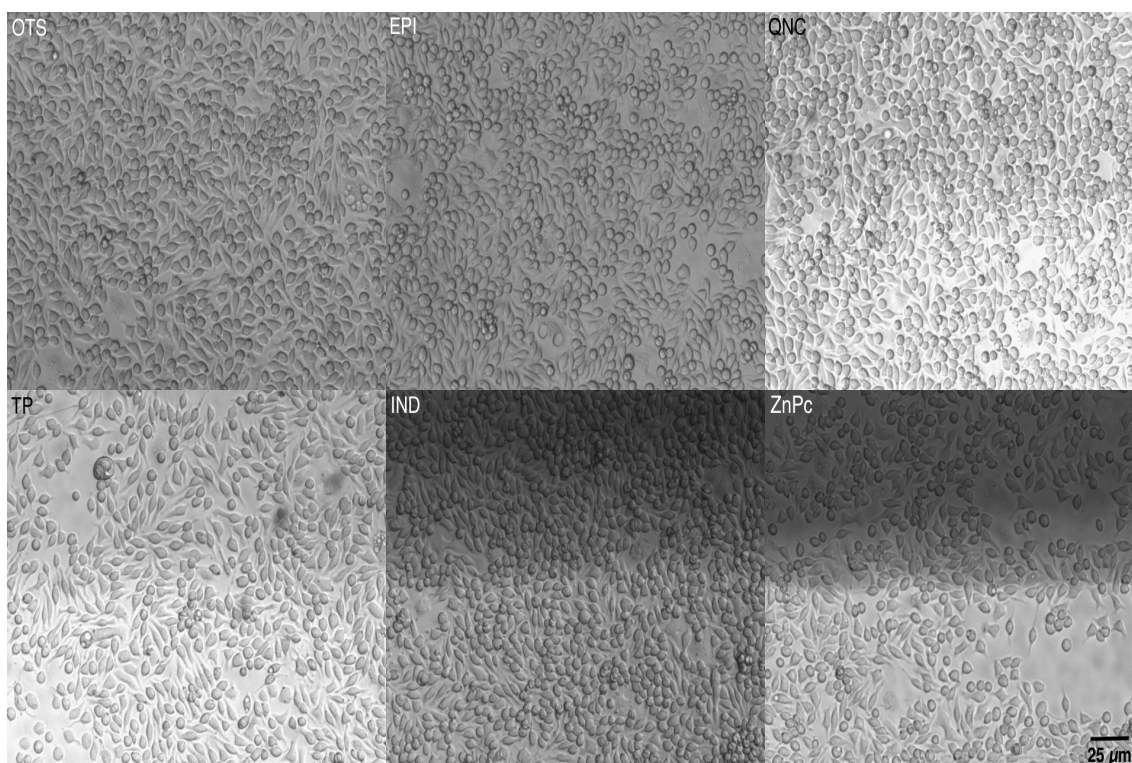


Figure 16: RBL cell growth on hydrogen bonded pigments thin films. OTS glass, EPI - Epindolidione, QNC - Quinacridone (top), TP - Tyrian Purple (top), IND - Indigo (top), ZnPc - Zinc Phthalocyanine (top).

3.2. Culturing cells on microcrystalline QNC structures

In the next phase of the experiments, hedgehog-shaped quinacridone microstructures, “jeziky”³² were immobilised onto the experimental substrates. The cultured cells, both RBL and HEK cells, showed preferential growth in contact with the microstructures. Figure 17 shows that the cells “reach out” towards the jeziky to establish a contact. In the case of HEK cells, this preference was maximized on OTS substrates, since HEK cells prefer more hydrophilic surfaces and OTS forms a hydrophobic monolayer. Thus for the patch-clamp experiments involving these cells, an alternative sticking layer had to be implemented. The objective was to find a suitable solution for both the HEK cells and the quinacridone microstructures to adhere to the surface. Ethoxylated polyethyleneimine proved to be a suitable candidate.

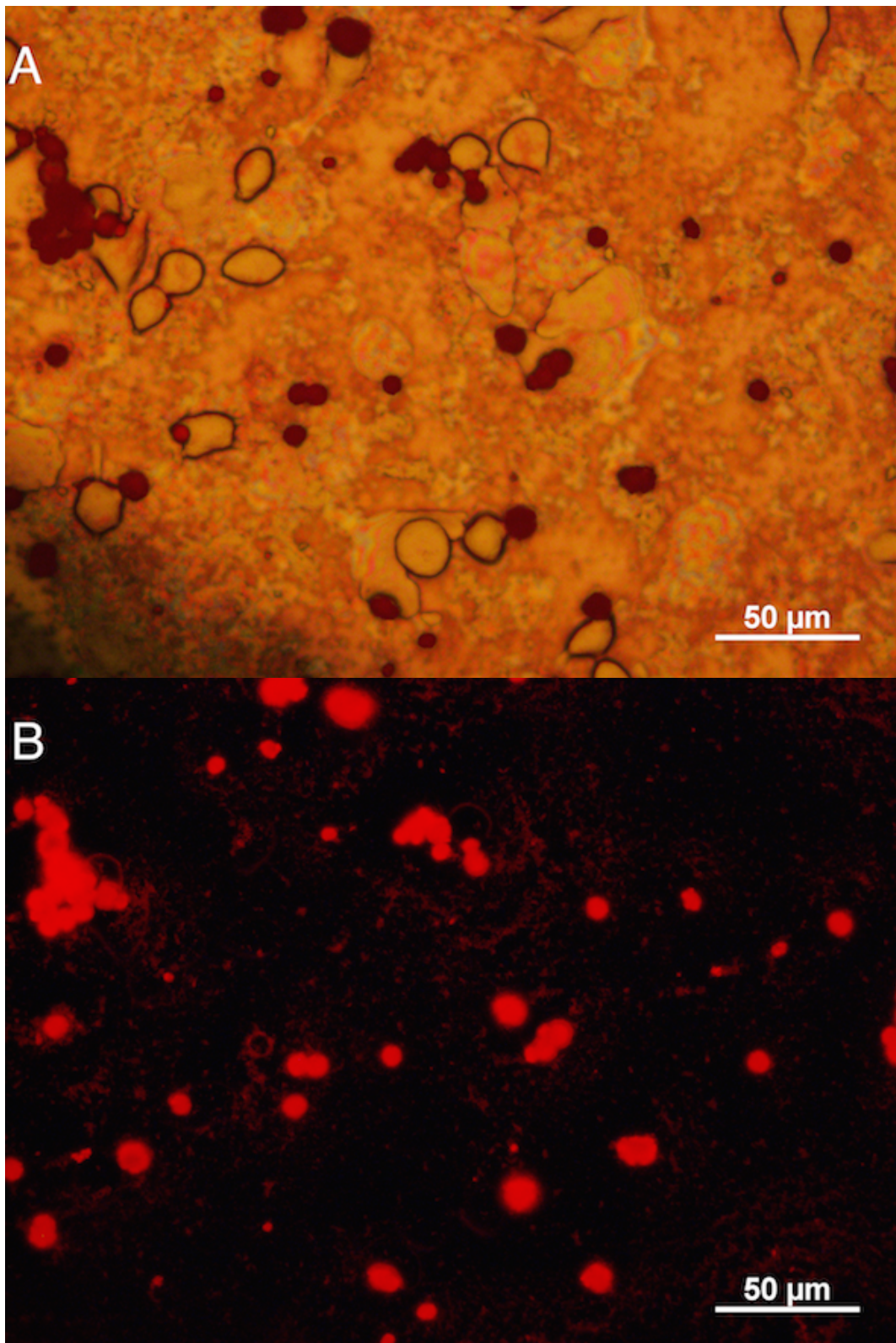


Figure 17: Microscope images of RBL cells cultured on OTS/Q479 jeziky substrates. A) bright field image, B) fluorescence image excited with green light

3.3. Patch clamp results for RBL non-specific voltage-clamp

After the compatibility of the cell culture with the pigments was confirmed, the next step included the investigation of an effect of the photo-excited semiconductors in the form of thin films on the ion permeability of cell membranes. For this purpose, whole cell voltage clamp measurements at a constant voltage -40, -20, 0, +20 and +40 mV were performed on RBL cells grown on substrates with thin films of the studied pigments. These were Zinc Phthalocyanine (ZnPc) and *N,N'*-Dimethyl-3,4,9,10-perylenedicarboximide (Me₂PTCDI) double-layers, indigo, tyrian purple (TP), quinacridone (QNC) and epindolidione (EPI). The double layer in both configurations were studied since the charging effects should be opposite and thus could deliver different results in the interaction with the cell. Various light sources corresponding to the absorption maximum of the semiconductor were used for excitation of the pigments; a 633 nm HeNe laser was implemented for indigo and TP, ZnPc/Me₂PTCDI and Me₂PTCDI/ZnPc double-layers, a LED emitting at 440-480 nm for EPI and a 532 nm diode laser for quinacridone, both of the above double-layers and P3HT. P3HT was used for purposes of comparison, since it was previously reported to exhibit a photoexcitation effect.³⁵ The cells were patched and the current was recorded at a given voltage. Once the cell was stabilized at a constant current value, the light irradiation was employed for a given time. The distinction between experimental and control cells is depicted in Figure 18. No pigment thin film, including P3HT, or control cell showed any effect *i.e.* increase or decrease in the current for any of the voltages applied (Figure 19).

Since the planar films showed no effect in the ionic currents of the cell, the structured quinacridone moieties, the jeziky, were employed. At that point, the first effects were observed (Figure 20). An increase of the current *i.e.* increase in permeability was observed depending on the polarity of the applied voltage. Structures of various size (2-4 μm and 8-12 μm in diameter) and branching were applied.³² The largest effect was observed for the larger structures of different branching patterns. It should be pointed out that such jeziky were on the same size order as the cells ($\sim 10\mu\text{m}$). The increase in permeability of the cells could be explained in two ways, either a certain ion channel activates thus causing influx/egress of ions in or out of the cell, or the membrane itself becomes unstable and leaky. Since the behaviour of the effect was depending on the polarity of the voltage, the response was not always reversible and the jeziky structures exhibit very sharp spines, the theory of increased leakage seemed more likely. Either the cell membrane could be penetrated by the structures already during culture, or the electric field concentration at point tips upon photoexcitation leads to the phenomenon of electroporation and hence disruption of the membrane. In order to resolve this question it was necessary to obtain a more detailed image of the cell/microstructure interaction/interphase, and to study a more defined membrane transport.

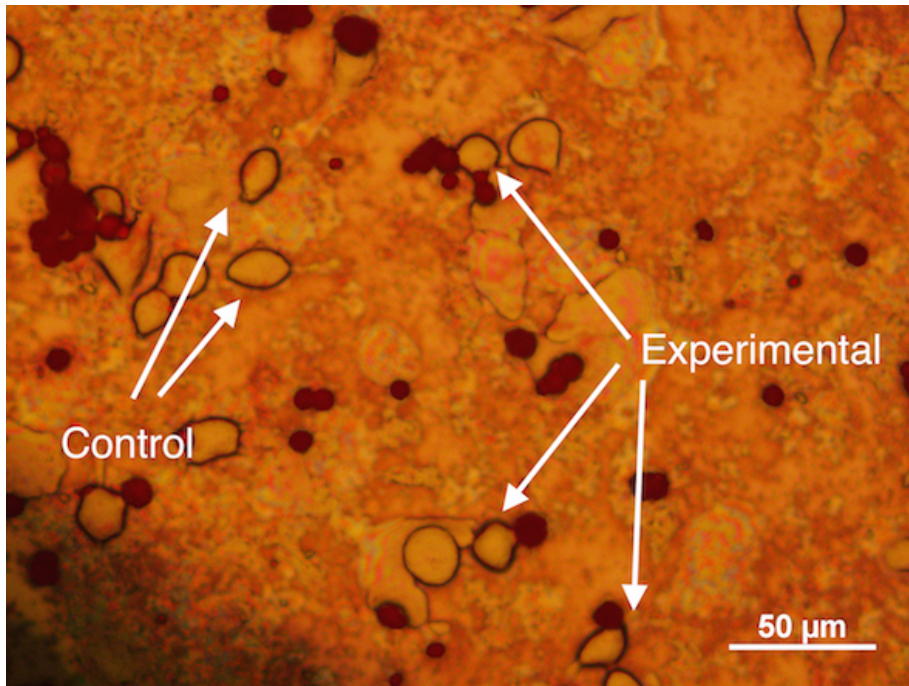


Figure 18: Distinction of control/ experimental cells in the experiments including quinacridone microstructures.

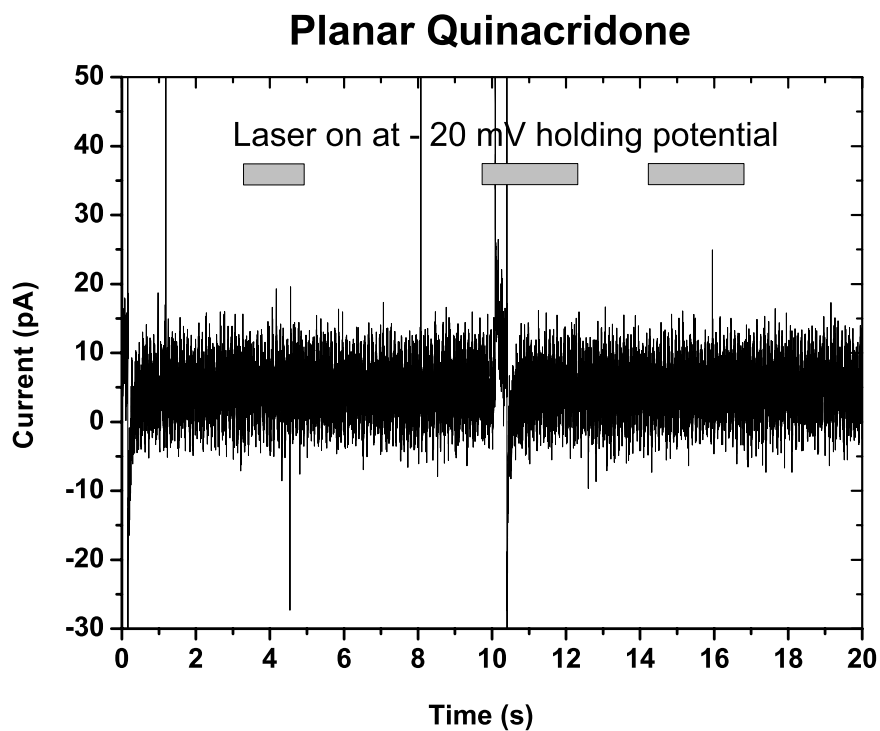


Figure 19: Voltage clamp at -20 mV of an RBL cell grown on a thin film of QNC with light on/off.

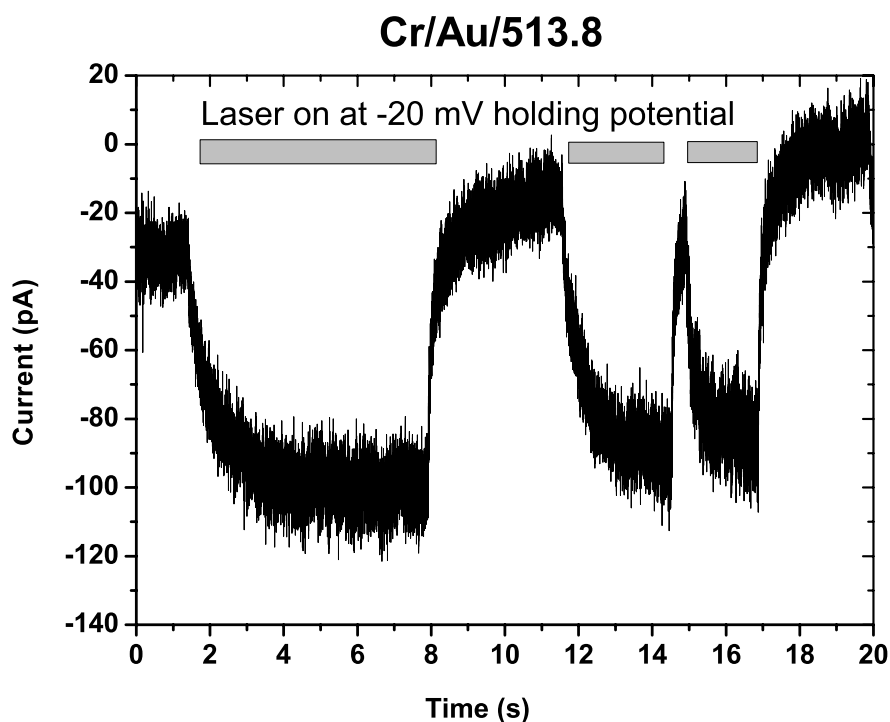


Figure 20: Representative voltage clamp at -20 mV of an RBL cell grown on a QNC microstructure with light on/off.

3.4. SEM investigation of QNC microstructures/cell interfaces for RBL and HEK

Since the cells of both of the cell lines appear to have intimate growth with the quinacridone microstructures based on optical micrographs, and the preliminary non-specific patch-clamp data indicated possible leakage, it was of interest to investigate the interface more closely. The microcrystal structure being on the order of several micrometers, but having sharp spines of approximately tenths of nanometers in diameter at the tip raised a question of possible disruption of the cell. Scanning electron microscopy was the technique of choice for such investigation. RBL and HEK cells were cultured on quinacridone microcrystals overnight / 4 hours respectively. In preparation for SEM, the cells were fixed with glutaraldehyde solution in PBS, dehydrated in a sequence of ethanol solutions and finally metallized with a film of gold. An intrinsic problem of the fixation/dehydration sample preparation sequence is substantial shrinkage of the cell volume (~20 %). This effect must be kept in mind when interpreting SEM images. In spite of this limitation, it was possible to deduce some valuable information. The RBL cells (Figure 21) showed that the cells indeed grow in an intimate contact with the microstructures. Surprisingly, the interaction of the cells with the quinacridone microcrystals was very strong, in cases stronger than the integrity of the crystal itself (Figure 21 C-E). In Figure 21 D,E it can be observed that the cell, retracting from the jezik due to shrinkage, extracts the needle-like crystallites from the jezik microcrystal body – signalling that the membrane/crystal surface interaction is stronger

than the integral forces holding together the crystal microstructure. From these images it also seems like no perforation of the cell membrane by the jeziky spines occurs, but rather that the cell membrane conforms closely with the nanostructured spines of the microcrystals. This is possibly due to the fact that the jeziky spines are terminated with hydrophobic alkyl chains, which engage in favourable hydrophobic-hydrophobic interactions with the hydrophobic fatty acids in the cell membrane. Definitive conclusions about perforation/penetration extent cannot be made without the use of a rigorous cross-sectional technique. The results, as expected, revealed that HEK cells prefer hydrophilic substrates (Figure 22), since when grown on OTS coated glass slides they grew exclusively on the jeziky microstructures. When PEI-E slides were used, HEK cells showed no preferential growth.

These findings were of a great interest since the question of cellular growth in close proximity with functional materials is widely investigated. It is generally accepted that planar substrates may not be ideal for the electrical coupling of the cells. Nanofabricated electrodes such as gold nanopillars, nanocavities or mushroom-shaped microelectrodes show an improved performance, however they still need an adhesive interlayer such as fibronectin thus forming an additional barrier between the active component and the cell.³⁶⁻³⁸ Other approaches designed electrode structures for intracellular recordings to penetrate cells without detrimental effects to the membrane.³⁹ The use of silicon nanowires or carbon nanotubes in cell recordings was also shown to be superior since the nanostructured surfaces promote cell adhesion even without the fibronectin interlayer and better electrical coupling.⁴⁰ Other groups further showed the use of microfabricated porous silicon nanoneedles/nanowires in direct delivery of particles such as quantum dots or plasmids inside of cells, which is based on the tightness of interaction between the cell membrane and the silicon structures, which are able to penetrate the membrane without any obvious damage.^{41,42}

In order to really study the direct interphase between the quinacridone structures and cells it would be necessary to obtain cross-sectional images. This would reveal the interaction and possible penetration of the spikes into the cell. This could be possible by using focused ion beam (FIB) during scanning electron microscopy to uncover lower layers of the sample. For this purpose, however, it would be vital to secure minimal contraction of the cell volume. Such result could possibly be obtained by using cryo methods or by freeze fixation with osmium tetroxide vapour. During the making of this thesis, steps were taken to make these methods available.

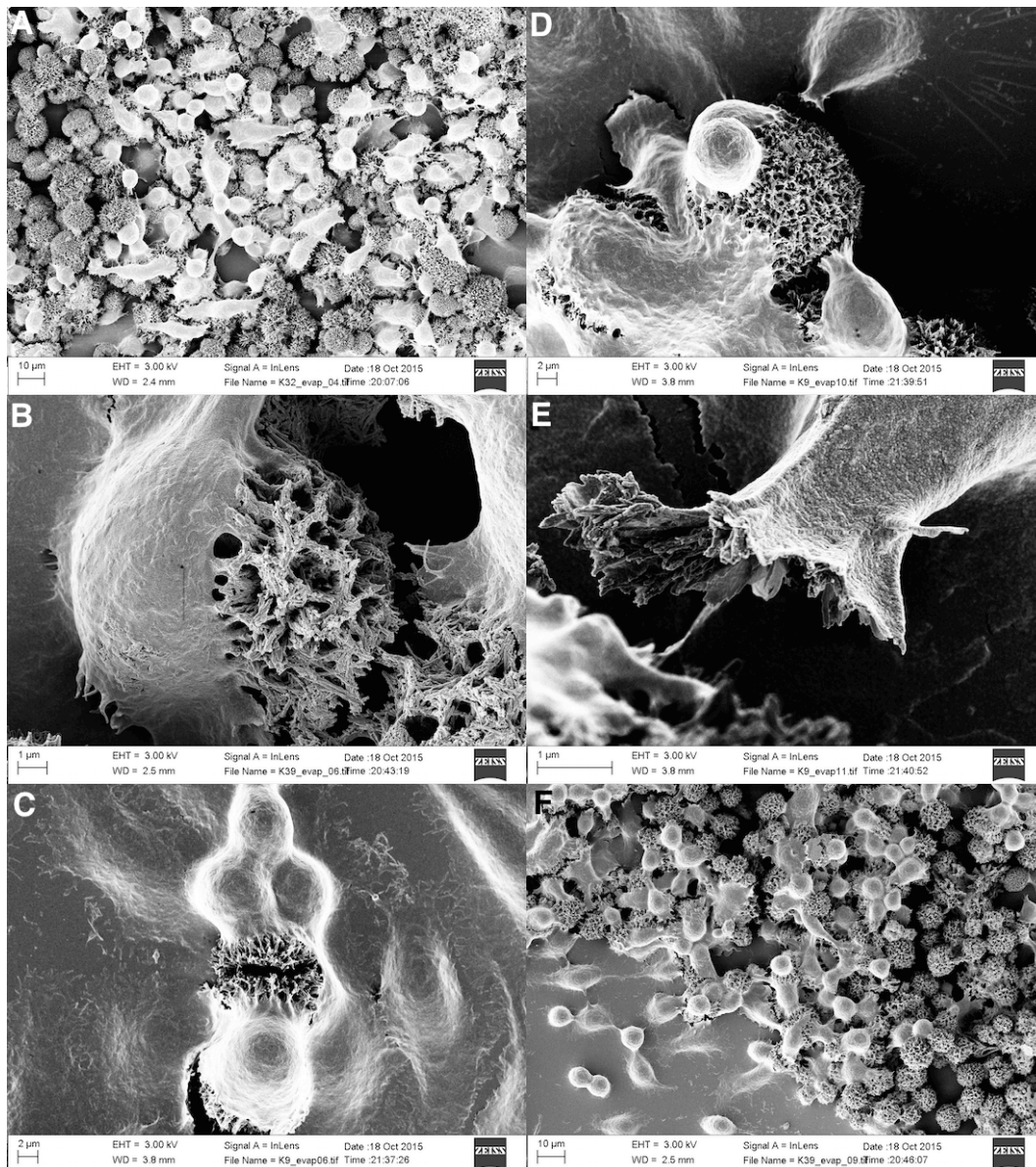


Figure 21: SEM micrographs of RBL-2H3 cell culture on OTS substrates with various quinacridone jazyky structures

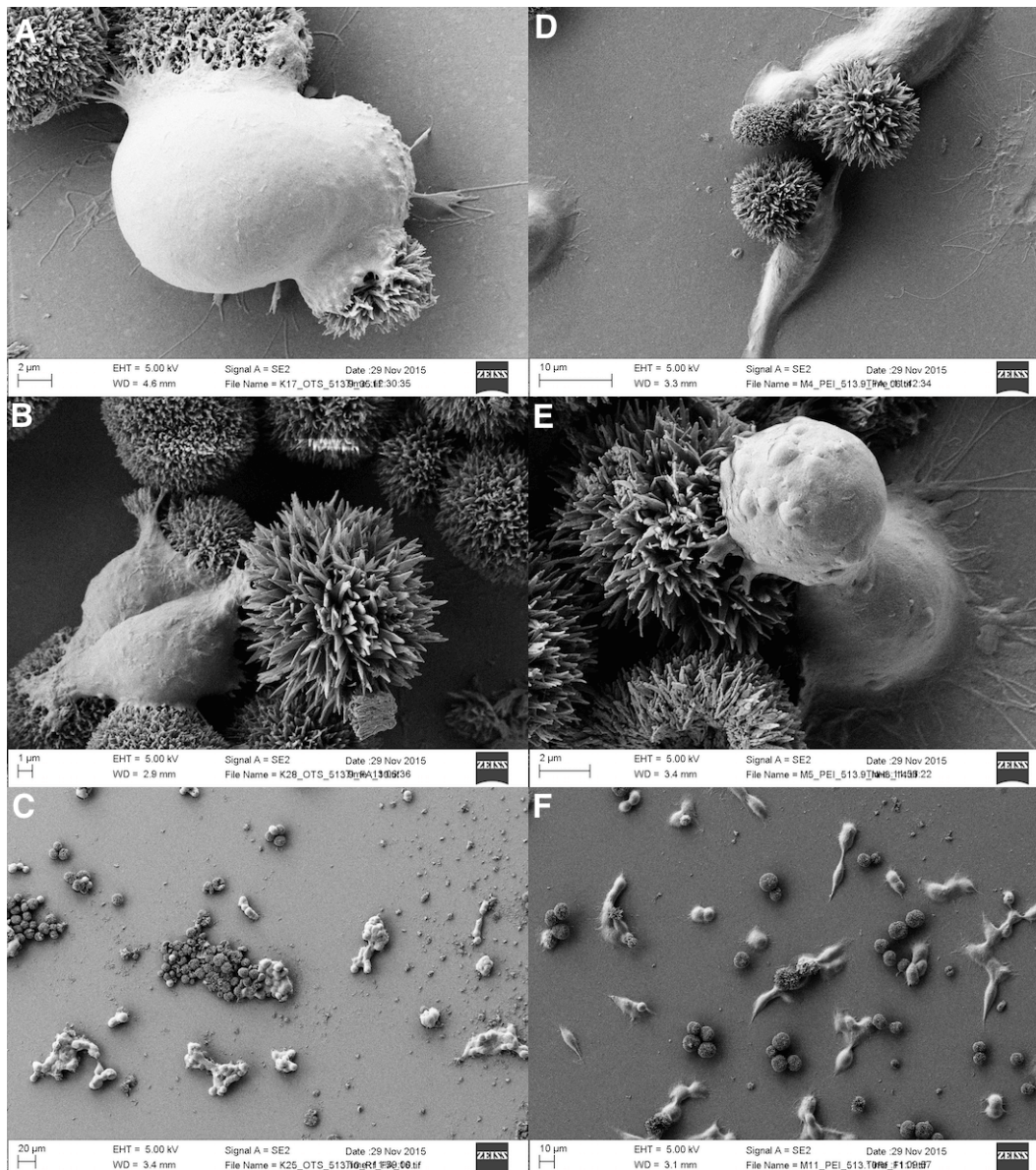


Figure 22: SEM micrographs of HEK293 cell culture on OTS (A,B and C) and PEI-E (D,E and F) substrates with various quinacridone jезiky structures.

3.5. Patch clamp results for K^+ inward rectifier in RBL cells

Inward rectifier K^+ channels are a family of membrane proteins which are important in establishment of resting membrane potential, regulation of neuronal, and cardiac electrical activity, controlling of glucose levels and of the overall ion homeostasis. The channel shows a diode-like behaviour in the sense that it is able to conduct much higher inward currents when the voltage of the membrane is more negative than the equilibrium potential, than in the reverse case. The channel conductance is dependent on the electrochemical K^+ potential. The rectification is caused by blockage of the channel in the outward direction by Mg^{2+} ions and polyamines such as spermine and spermidine.^{43,44} It has been reported that the potassium inward rectifier is the only voltage-dependent ion channel present in RBL cells under normal recording

conditions.^{25,45} Thus studying of this channel in RBL cells was an ideal candidate to determine the nature of the activation caused by laser irradiation. By studying the K^+ inward rectifier specifically, one can discriminate if light irradiation causes membrane leakage or if it truly affects channel activity. If the rectification characteristic of ion flow is preserved upon irradiation, nonspecific membrane leakage can be excluded.

In our experiments, voltage ramps between -120 mV and +60 mV lasting for 100 ms were applied from a holding potential of 0 mV and were recorded continuously. The laser irradiation was applied after a constant reliable signal was observed in dark. A cell was considered “experimental” when at least one semiconductor microstructure was in contact with it. Those not in direct contact are considered “control”. In order to compare the effects of laser irradiation on potassium inward rectifier in RBL cells, the maximum value of activation (maximum negative current, typically around -115 mV) was determined for each voltage ramp. Figure 23 shows a typical recorded plot in case of increased activation, which indeed confirms the hypothesis that the light-induced effect is not simply electroporation-like, because the channel retains its rectifying property by enhancing the signal only at certain voltage range while staying constant otherwise. The graph shows that the time scale of the light enhancement is on the order of hundreds of milliseconds since it is necessary to record several ramps in order to reach the maximum current. Furthermore one can deduce that the activation is reversible because the dark curves before and after laser irradiation overlap. The maximum activation in terms of maximal negative current was then normalized to the value of current in ambient light conditions and plotted as a function of time. Figure 24 shows such a plot for an example of the quinacridone microstructure (433.9_Rf/Cr/Au). The activation observed occurs over the timescale of hundreds of milliseconds, reaching a plateau after a few seconds. It was also found that the normalized enhancement is variable among the experimental cells of the same kind. This behaviour was reproducible over wide variety of microstructure types, the absence/presence of riboflavin ligand and metal layers. The results were summarized in terms of % increase in the activation current (Figure 25). All the experimental cells showed higher activation in comparison to the control, however, the variation among the cells of the same experimental group were large given by the varying number of microstructures in contact and the cell size. One of the conclusions which could be drawn from the data is that the layer design with various metal layers on top of the semiconductor structures showed higher increase when compared to the naked structures or structures deposited on Cr/Au layer. The fact that all designs produced similar effects with rather slow dynamics of the light-enhanced phenomena was indicating that the possible mechanism could be photothermal heating. To further investigate such a hypothesis, substrates covered with areas of carbon black were included in the study. Carbon black is a conductive and not a semiconducting material, thus any observable light effect should be attributed to heating. As shown in Figure 25 and 26, the behaviour of carbon black samples was similar to those of the quinacridone microstructures. In addition, Figure 26 shows the effect of lowering the laser output power by applying optical density filters on the activation of the channel. Taken together, the results point to the conclusion that the mechanism for light-induced enhancement of K^+ inward rectifier ionic currents was photothermal in nature.

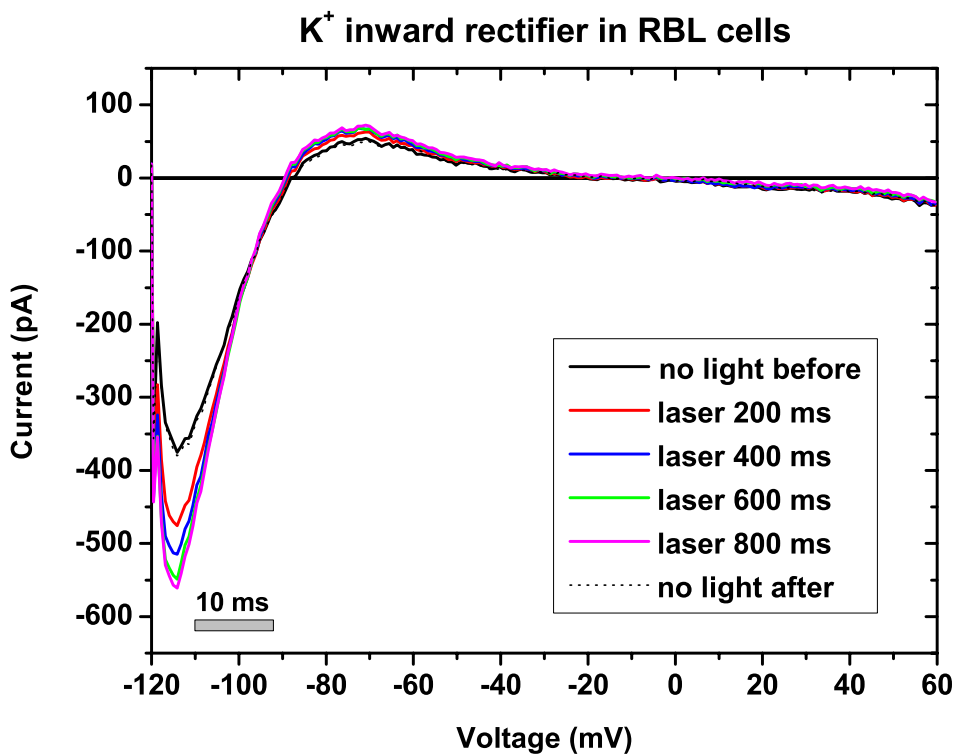


Figure 23: Recording settings for potassium inward rectifier in RBL cells. Grey scale bar shows the relationship between the time and applied voltage during the experiment, each ramp lasts 100 ms.

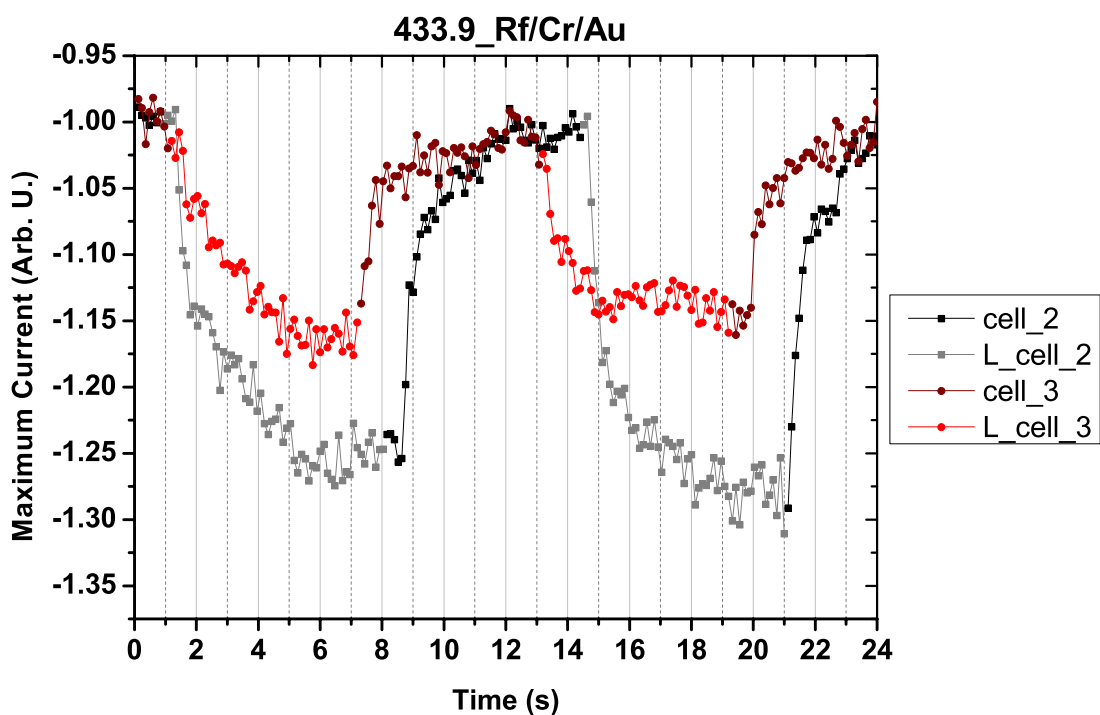


Figure 24: Typical plot of the maximum activation current normalized to the base line value as a function of time. Two different cells of the same experimental groups are depicted. “L” stands for laser illumination period.

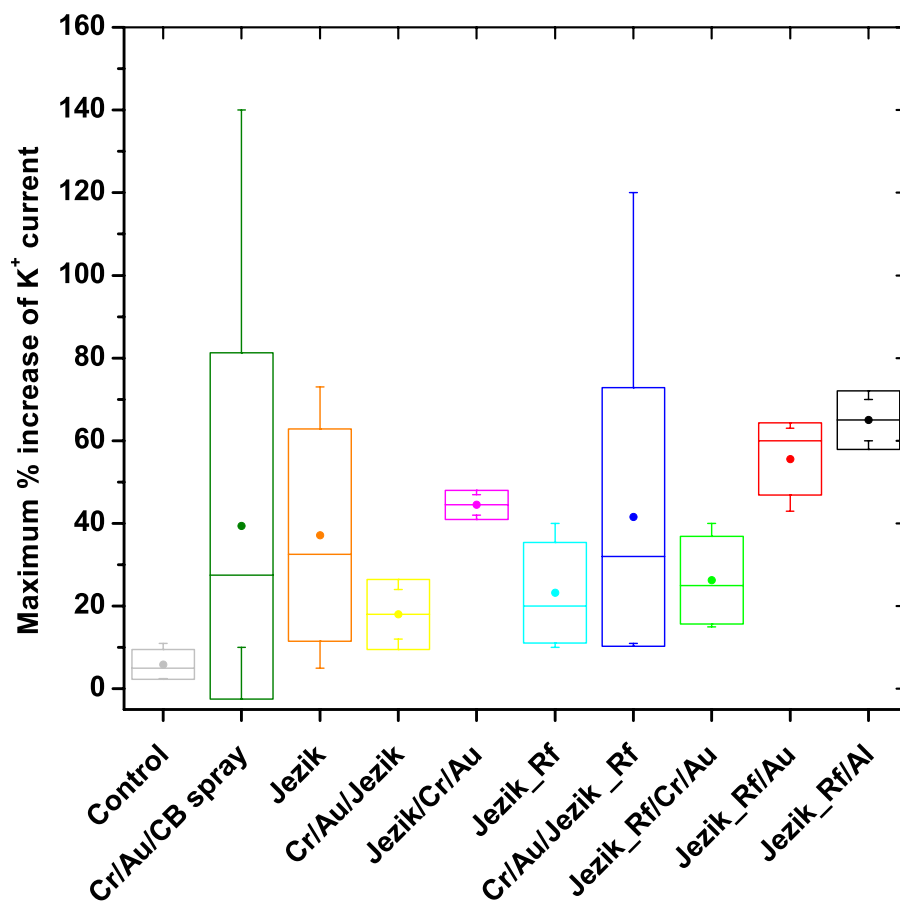


Figure 25: Comparison of the effect of laser irradiation on the maximum activation current. Jezik stands for various quinacridone microstructures. The sides of the box plots indicate SD, the dots the average values and the whiskers the maximum/minimum (n = 2-14).

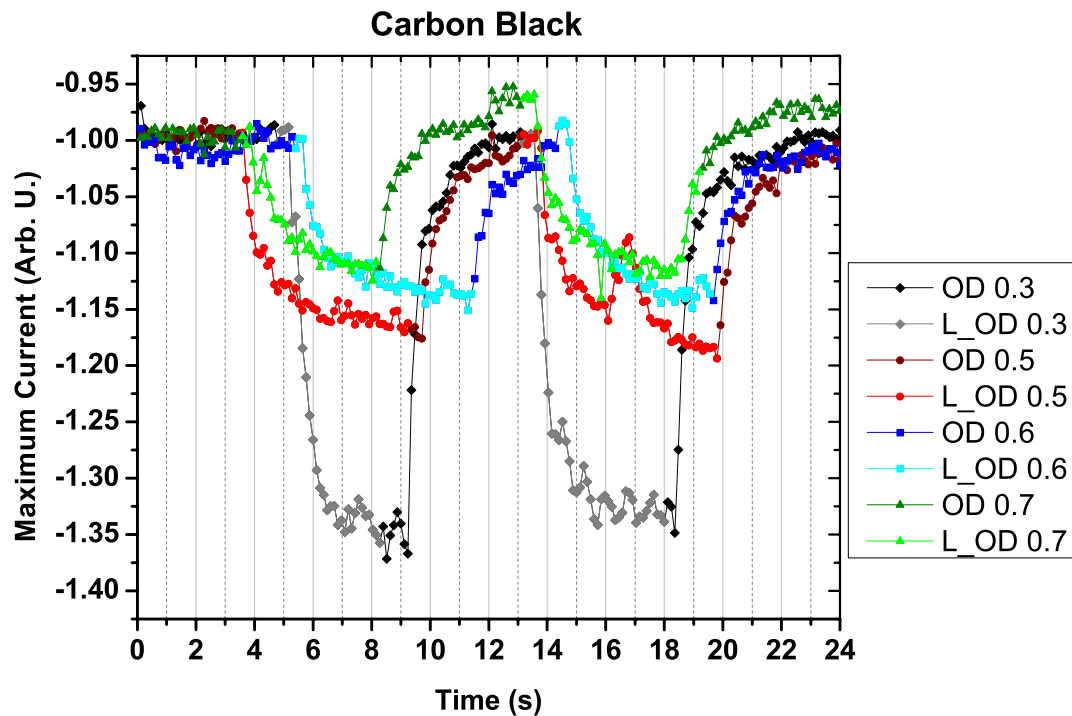


Figure 26: Plot of the maximum activation current in carbon black samples. A single cell exposed to various light intensities. "L" stands for laser illumination period, "OD" for optical density filters.

3.5.1. Single channel analysis of K^+ inward rectifier in RBL cells

Since there was observed a clear increased activation of potassium inward rectifier channels on the whole-cell level, it was endeavoured to investigate the behaviour of single channels. For this purpose the cells were kept in the cell-attached mode and held on the resting potential value. Twenty swipes lasting for 2 seconds were recorded for each cell with the laser irradiation on for selected swipes. Figure 27 shows a typical measurement for cells in contact with the quinacridone structures. The channel opening time and number of open channels seem not to be perturbed upon laser irradiation, however, the amplitude of the current is slightly higher when the laser is on. This phenomena could be caused by increased influx of ions due to heating, although a voltage shift causing higher activation of the channel is also possible.

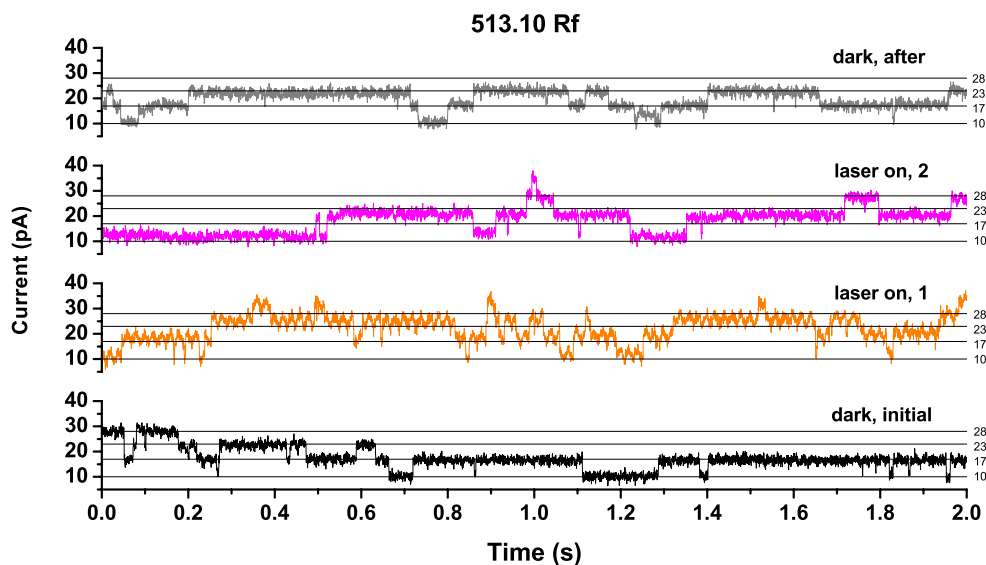


Figure 27: Single channel measurements for K^+ inward rectifier. Swipes with laser irradiation are depicted in orange and pink.

3.6. Patch clamp results for L-type Ca^{2+} voltage-gated channels in HEK cells

L-type Ca^{2+} voltage gated channels exhibit large voltage activation, slow voltage-dependent inactivation, and high single channel conductance. These channels participate in neurotransmitter and endocrinal release, regulation of gene expression, initiation of muscle excitation, and sensory cell signalling including retinal neurons, all of which are triggered by cell depolarization and subsequent influx of calcium ions into the cell interior.^{46,47} In order to determine if quinacridone jeziki can effect changes in voltage-gating upon photostimulation, the L-type calcium voltage-dependent channel, α and β subunit were overexpressed in HEK293 cell line.

In order to further discriminate if the effects visible were of a capacitive origin, the jeziki were coated with either a low- or high-work function metal. $Cr_2O_3/Cr/Au$ was chosen as the low-work function contact, as it has been shown to be an environmentally-stable low-work function contact.⁴⁸ Gold alone was used as the high work function contact (Figure 28) Since QNC is known to be an ambipolar semiconductor in principle the creation of both an n-type or p-type depletion layer should be possible, and may result in opposite capacitive surface charging upon photoexcitation.⁴⁹ Even if this is not the case, the energetic differences arising from the significant difference in work function of the two metallic coatings could manifest itself in the gating of a voltage dependent channel. Constant voltage recordings were performed between -50 mV up to 100 mV in 10 mV steps each lasting for 300 ms. The activation of the channel was first determined in dark and then the full sequence was recorded under illumination. The same activation was observed in both types of metal coatings, upon photoexcitation the amplitude of the current increased and the maximum activation voltage shifted to more negative voltages (Figure 29-31). The coating was conducted using vacuum evaporation, which probably did not give adequate conformal coverage, however a larger statistical sample would be

needed. Furthermore, riboflavin structures were employed because it has been previously shown, that it acts as electron acceptor and that QNC is able of charge transfer towards riboflavin upon photoexcitation.³² Since all the structures and coatings delivered the same results, it was concluded that this is further evidence for the photothermal effect being the dominant mechanism behind the observed channel behaviour.

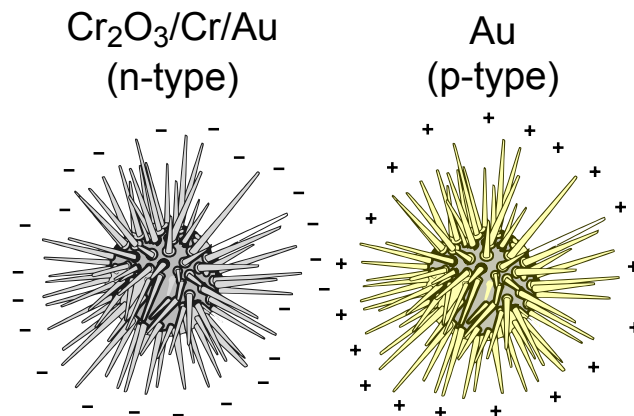


Figure 28: Proposed mechanism of microstructure transient photocharging by applying different coating

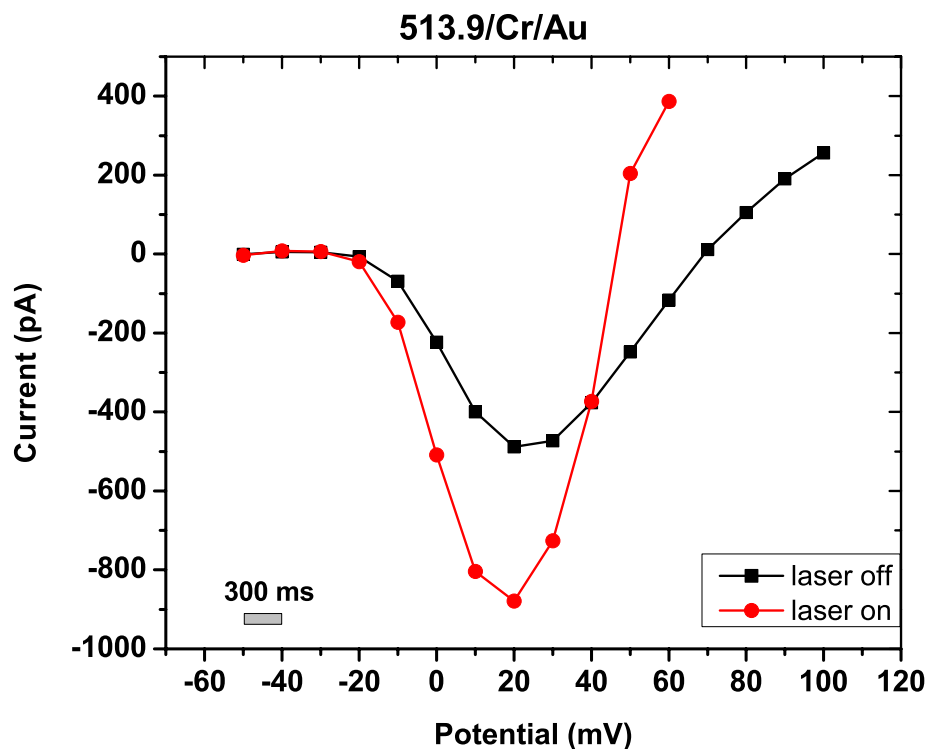


Figure 29: Calcium voltage gated ion channel in HEK293 cells. Cr/Au coating of the QNC structures.

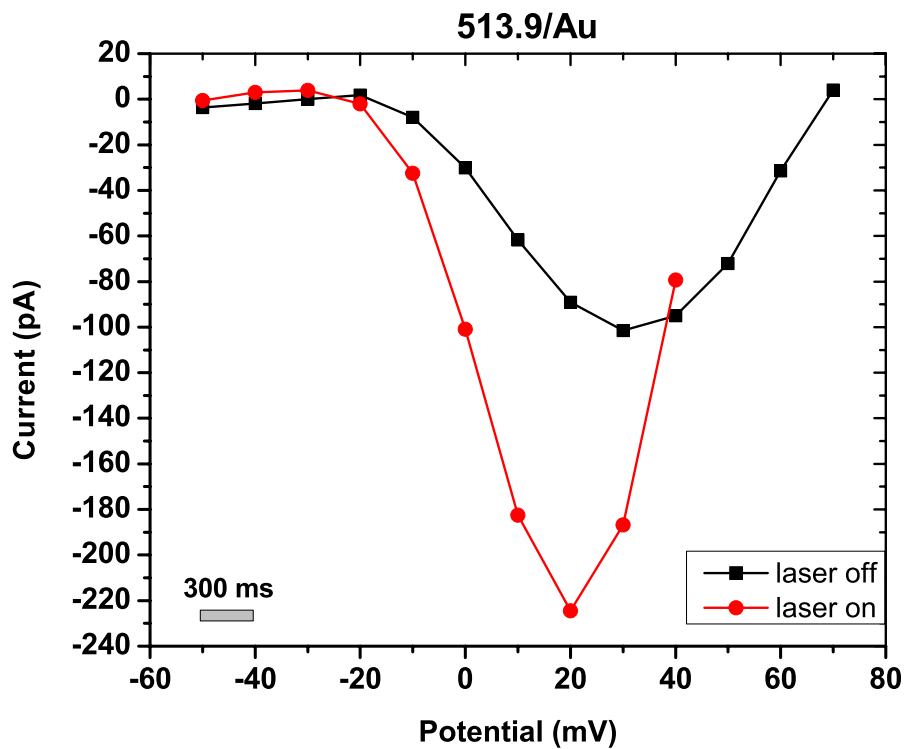


Figure 30: Calcium voltage gated ion channel in HEK293 cells. Au coating of the QNC structures.

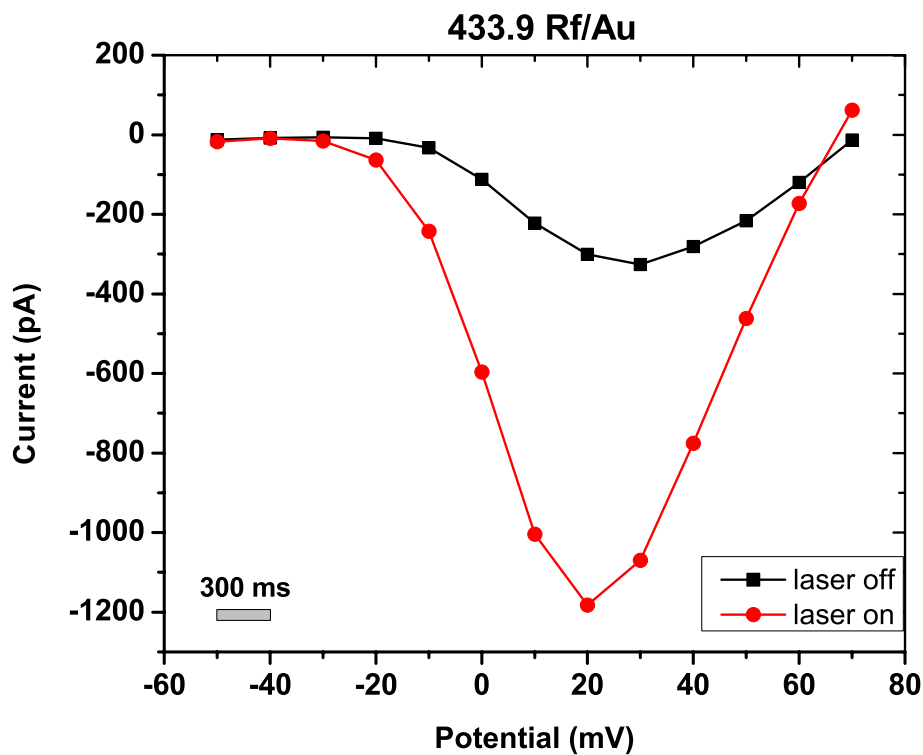


Figure 31: Calcium voltage gated ion channel in HEK293 cells. Au coating of the QNC structures with riboflavin.

3.7. Patch clamp results for temperature-gated channel TRPV1 in HEK cells

The transient receptor potential vanilloid subfamily (TRPV) ion channels have been identified as temperature-gated ion channel. The general role of the non-selective cation TRPV1 channel is in the inflammatory response and transduction of pain. These channels respond to activators like capsaicin, heat, and lowered pH. The threshold for rapid activation of the channel is about 40°C. However, the mechanism behind the heat activation is not yet solved.⁵⁰⁻⁵² TRPV channels have been shown to be addressable with direct IR laser stimulation of water molecules,⁵³ or by IR-absorbing semiconductor polymer nanoparticles heated by a 880 nm laser.¹² In order to further elucidate the mechanism of the light induced activation of cells in contact with the jeziky microstructures, the TRPV1 channel was transfected into HEK293 cells.

A typical measurement is depicted in Figure 32. The channel saturates already after the first ramp, thus the maximum light-induced activation is reached within 200 ms. For further purposes the maximal current (at applied voltage of +100 mV) was plotted as a function of time and was normalized to the current before first laser irradiation. Figures 33-35 show the transients for a control, one jezik type and a carbon black control respectively. The control on plain glass indicates that laser irradiation by itself is not sufficient for the channel activation, while an introduction of warm solution (rise of temperature by ~1°C) showed a small fluctuation. In the case of the other probes, laser-induced activation was observed, which was rather reversible in case of the microstructure, while in case of carbon black treated substrate, the activation typically lead to cell death. These results strongly indicate that heating is the main cause of the activation, however, it should be noted, that changes in pH and membrane polarity are also reported to affect the gating properties of TRPV1 channel.⁵¹

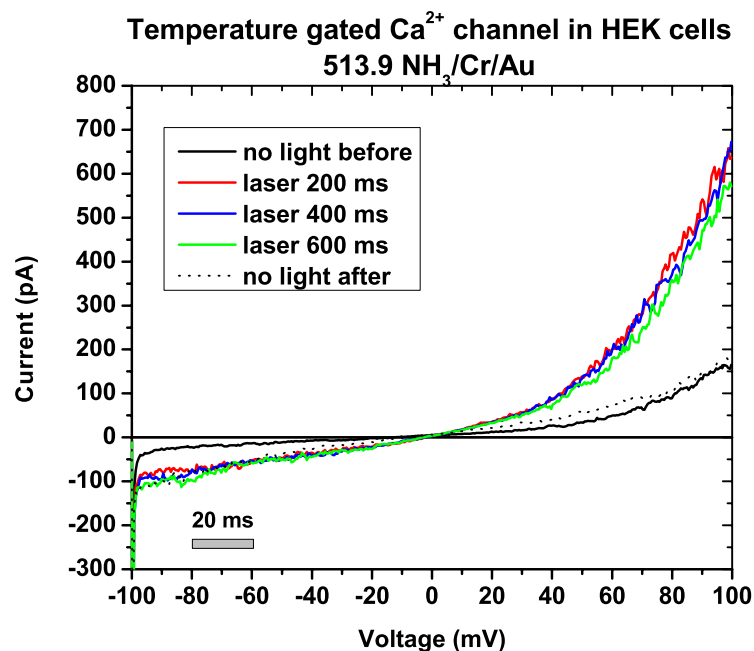


Figure 32: Current-voltage relationship for TRPV1 overexpressed in HEK cells in response to light illumination. Grey scale bar shows the relationship between the time and applied voltage during the experiment, each ramp lasts 200 ms.

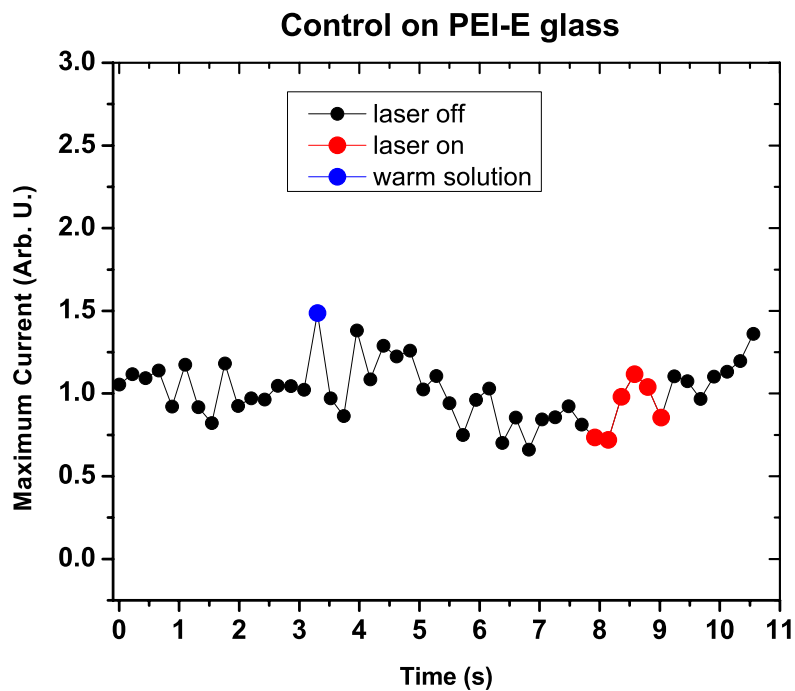


Figure 33: Plot of a typical time course experiment showing maximum TRPV1 current normalized to the baseline in the control HEK cell experiment.

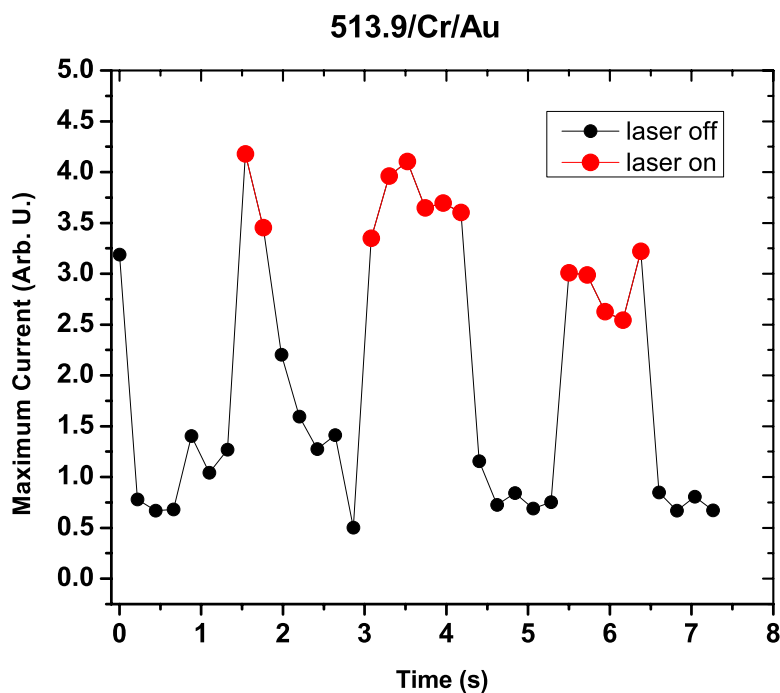


Figure 34: Time-course of maximum TRPV1 current normalized to the baseline in a HEK cell in contact with the jezky structures.

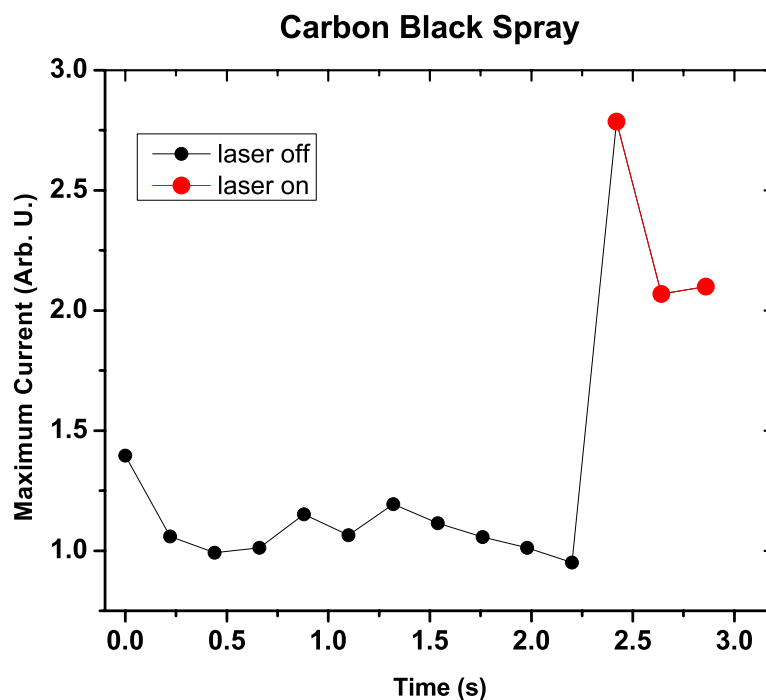


Figure 35: Time-course of maximum TRPV1 current normalized to the baseline in a HEK cell on a carbon black substrate.

3.8. Measurement of local laser-induced heating using calibrated pipette

Since most of the data pointed towards photothermal mechanism of the cellular activation when in contact with the semiconductor microcrystals, the local probing of temperature was introduced in order to determine the extent of heating upon laser illumination. A calibrated pipette method was used for the local measurements as described in the methods section.^{11,50} The pipette current showed a linear relationship with the measured temperature in the range of room temperature + 10°C (Figure 36). The method was then used to determine the laser irradiation induced current. Figure 37 shows typical responses of the pipette currents to the laser illumination, heating of about 1°C resulted in both the temperature control carbon black samples and in various jeziky probes. The results further indicate, that the transient behaviour is similar in both cases that the extra layer of Cr/Au increases the temperature effect by ~50% and that the behaviour is dependent on the laser power *i.e.* optical density filter applied. Figure 38 indicates that the heating is comparable in all kinds of substrates including the jeziky microstructures, carbon black, or the planar films of QNC and P3HT and is approximately 1°C when using the laser with a 0.3 OD filter (as was used throughout all cell stimulation measurements presented). The exception is the Cr/Au/jezik Rf probe, which shows larger degree of heating, this might be caused by a slightly thicker Cr/Au layer, since in that case the reflection of the light would account for the extra heating. The results also show, that the presence of Cr/Au layer is sufficient for considerable heating, the amplitude is, however, hard to quantify, since it was not possible to determine the exact position of the laser irradiation spot due to strong reflection. It is worth mentioning, that the temperature was probed in the vicinity of the quinacridone

structures, not in direct contact. Considering that Martino et al. observe similar absolute rise of $\sim 2\text{-}3^\circ\text{C}$ when applying the method to thin films of P3HT,¹¹ while the temperature increases in case of IR laser mediated heating of water molecules are an order of magnitude larger,^{50,54} it is possible to compare the efficiency of the various probes, however this technique does not provide means of estimating the real temperature at the crystal/cell interface. In order to estimate the true temperature profile, it would be necessary to employ such method while changing the distance of the pipette from the structure precisely on a micrometre scale and modelling the interface from the obtained data, or by applying a high resolution IR camera.

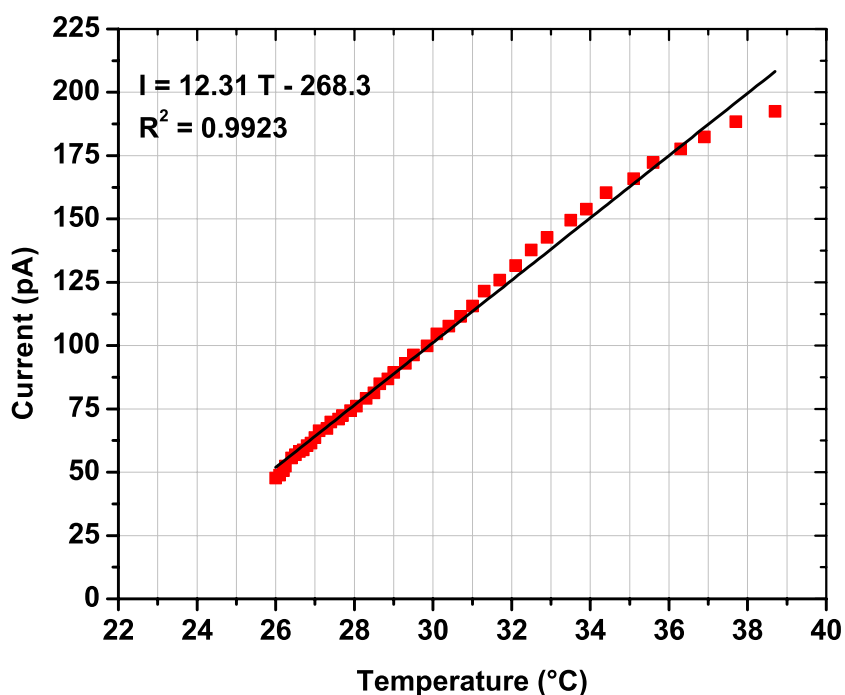


Figure 36: The calibration curve for temperature dependence of the pipette current.

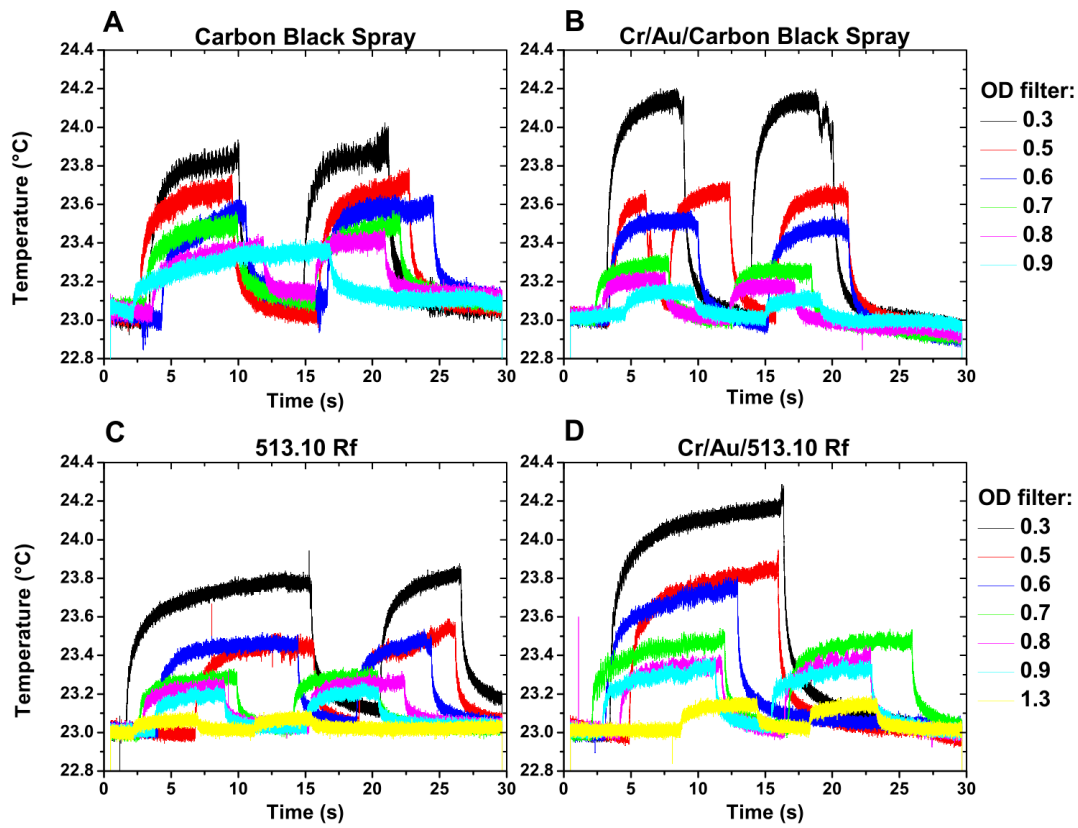


Figure 37: Locally probed temperature increase induced by laser irradiation and its dependence on the attenuation of the laser power.

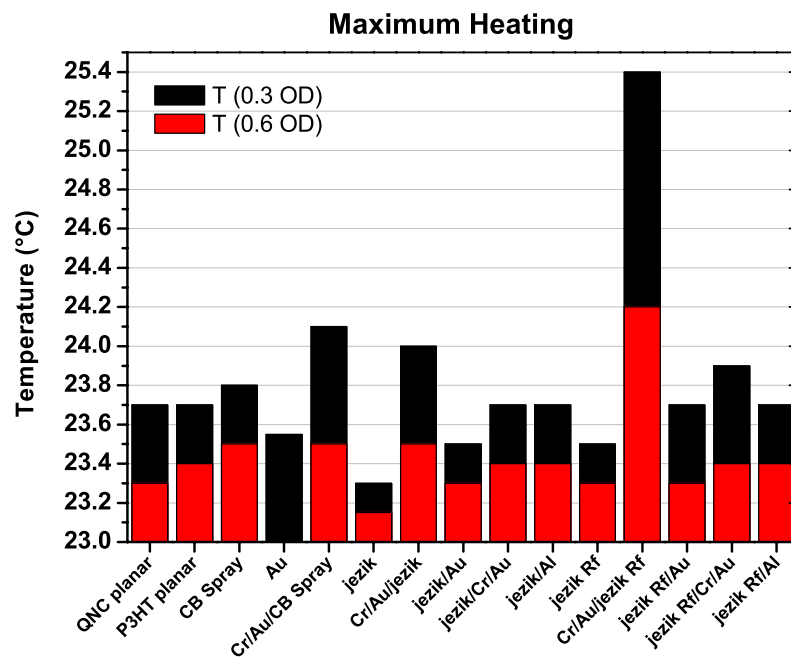


Figure 38: Overview of the maximal heating of different layer deposition configurations.

3.9. (Photo)electrochemistry of jeziky, hydrogen peroxide

The quinacridone material, as the other reported hydrogen-bonded semiconductors, exhibits a reversible 2 electron oxidation and reduction.²⁹ It has been recently shown, that QNC is able to perform 2-electron photoreduction of oxygen dissolved in water solutions. The product was proven to be hydrogen peroxide just by the end of the period dedicated to this thesis.⁵⁵ This finding raised the question of the possible role of the third mechanism mentioned in the introduction section – Faradaic processes.

In order to test this possibility, electrochemistry of the quinacridone structures was measured. QNC jeziky deposited on Cr/Au electrode were used as working electrode, platinum wire as counter electrode and Ag/AgCl as reference electrode. Figure 39 depicts chronoamperometry of the QNC structures in various solutions, including the extracellular solution used in patch-clamp measurements. Clear photocurrent, corresponding to formation of H₂O₂, was observed in all cases. In order to test the hydrogen peroxide formation in conditions more similar to the patch-clamp measurements, the concentration of H₂O₂ was measured as function of time in samples of extracellular solution, which was in contact with the QNC jeziky and was irradiated by halogen lamp (intensity 50 mW/cm²). The amount of formed peroxide was followed by the TMB/HRP assay using the end-point method as specified in the methods section. Figure 40 shows, that after 10 min of constant irradiation, hundreds of picomoles of H₂O₂ are formed corresponding to ~1-10 μM. Since the irradiation times in the patch-clamp measurements are much shorter and the amount of possible H₂O₂ formed should be even lower, this is far from the concentrations reported to affect any kind of ion channel activities.^{21,56,57} Thus it is not likely, that the effects observed in the previous sections are due to the photoelectrochemistry of the structures, despite it is to be considered in case of long-term studies and or possible applications in prosthesis development.

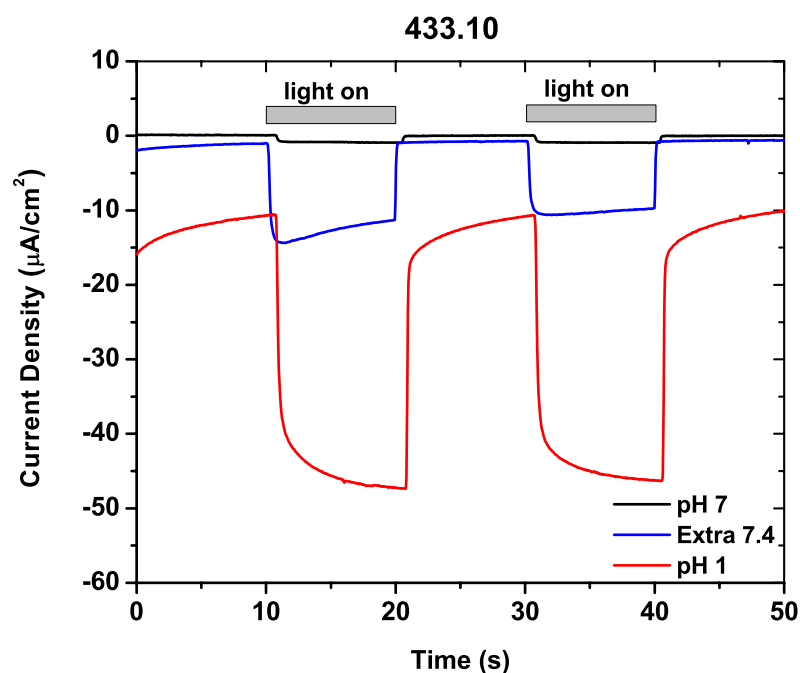


Figure 39: Chronoamperometry of jeziky photocathodes at 0V vs. Ag/AgCl in pH 1, pH 7 and 0.3 Ca²⁺ extracellular solution.

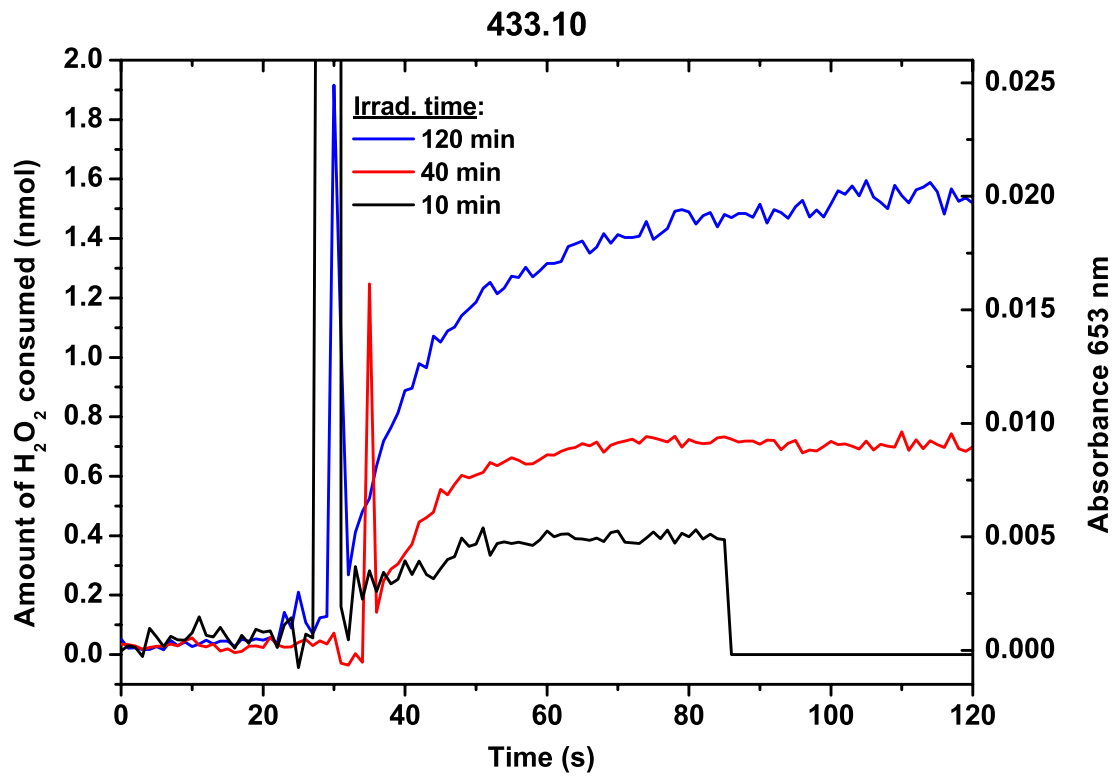


Figure 40: The quantification of hydrogen peroxide formation in the 0.3 Ca²⁺ extracellular patch-clamp solution after 10, 40 and 120 min of irradiation.

4. Conclusion

The use of hydrogen-bonded semiconductor microstructures showed consistent and reversible photostimulation of rat basophilic leukemia cells and transfected human embryonic kidney cells. The reason for efficient activation is probably the close proximity of structure-cell interactions as proven by scanning electron microscopy. The biomimetic nature of quinacridone crystals causes the cells to adhere well even in the absence of an interlayer coating.

In order to elucidate the mechanism of the activation, several ion channels were studied. These included intrinsic potassium inward rectifier in RBL, and transfected L-type voltage gated calcium channels with temperature dependent channels in HEK293 cells. Increased activation upon laser illumination was observed in all cases. It should be taken into account that the experiments performed on HEK cells were not statistical and results that were at least once reproducible were presented herein. The reason is, that it was difficult to obtain larger amounts of data due to limited number of cells, which exhibited all necessary conditions for measurements *i.e.* contact with jeziky, sufficient fluorescence level for confirmation of channel expression, and successful activation of the channel. In order to obtain statistically relevant data, the latter two could be approached by transfection optimisation for the purpose of future studies. Nevertheless the presence of activation also in carbon black treated substrates acting as a temperature effect control supported the hypothesis of photothermal mechanism. It was proven using an *in situ* electrochemical method that the local temperature in proximity of the structures or carbon black structures increased by $\sim 1-1.5^{\circ}\text{C}$ during illumination, the estimation of the temperature at the real cell/crystal interface remains to be studied.

The mechanism behind thermal effect is not fully known; it could include stimulation of thermally activated ion channels, increased channel conductance, decrease in Nernst equilibrium potential, formation of a transmembrane pore or a combination of them.^{18,19} Based on the results presented in this thesis, we propose that the most probable mechanism for activation is that heat induces higher rate of ionic exchange thus increasing the conductance of the channels, since activation was observed in different channels of opposite functionality (potassium K^+ inward rectifier activates upon hyperpolarisation, while voltage dependent Ca^{2+} channel CAL upon depolarisation). Faradaic processes including hydrogen peroxide are possible, however they should not dominate on the timescale of the performed patch-clamp measurements. It is, however, important to consider them in any kind of longer-term studies or longer-term photoeffects. It is very likely that all three mechanisms take place at the same time during the photostimulation of cells, in which case it is very hard to distinguish between their individual effects. It is definitely worth to study each separately, if possible, to determine their limitations and hazards and to then optimize the active structures accordingly.

Pure thermal activation, which is highly specific, is of considerable practical interest. Some of the technologies used in retinal implants are based on local heat activation by infrared lasers.⁵⁸ However, the IR-laser induced neuronal activation is usually limited by the necessity of local light delivery by optical fibers, since the maximum penetration

depth is on the order of 100-1000 micrometers. Thus an alternative using a direct injection of specific microcrystals directly in place of damaged photoreceptors would be promising, since the spatial resolution could be increased. For similar reasons the microparticles could be applied in *in vitro* thermal studies of cellular behaviour or for photodynamic therapy in case of specific labelling of the structures to target cancer cells.

5. References

1. Bareket-Keren, L. & Hanein, Y. Novel interfaces for light directed neuronal stimulation: Advances and challenges. *Int. J. Nanomedicine* **9**, 65–83 (2014).
2. Ghezzi, D. Retinal prostheses: progress toward the next generation implants. *Front. Neurosci.* **9**, 1–6 (2015).
3. Bongo, M. *et al.* PEDOT:gelatin composites mediate brain endothelial cell adhesion. *J. Mater. Chem. B* **1**, 3860 (2013).
4. Colicos, M. A., Collins, B. E., Sailor, M. J. & Goda, Y. Remodeling of Synaptic Actin Induced by Photoconductive Stimulation. **107**, 1–12 (2001).
5. Goda, Y. & Colicos, M. a. Photoconductive stimulation of neurons cultured on silicon wafers. *Nat. Protoc.* **1**, 461–467 (2006).
6. Suzurikawa, J. *et al.* Light-addressable planar electrode with hydrogenated amorphous silicon and low-conductive passivation layer for stimulation of cultured neurons. *Annu. Int. Conf. IEEE Eng. Med. Biol. - Proc.* **93901**, 648–651 (2006).
7. Starovoytov, A. *et al.* Light-Directed Electrical Stimulation of Neurons Cultured on Silicon Wafers Light-Directed Electrical Stimulation of Neurons Cultured on Silicon Wafers. *J. Neurophysiol.* **93**, 1090–1098 (2004).
8. Ghezzi, D. *et al.* A hybrid bioorganic interface for neuronal photoactivation. *Nat. Commun.* **2**, 166 (2011).
9. Ghezzi, D. *et al.* A polymer optoelectronic interface restores light sensitivity in blind rat retinas. *Nat. Photonics* **7**, 400–406 (2013).
10. Gautam, V., Rand, D., Hanein, Y. & Narayan, K. S. A polymer optoelectronic interface provides visual cues to a blind retina. *Adv. Mater.* **26**, 1751–6 (2014).
11. Martino, N. *et al.* Photothermal cellular stimulation in functional bio-polymer interfaces. *Sci. Rep.* **5**, 8911 (2015).
12. Lyu, Y., Xie, C., Chechetka, S. A., Miyako, E. & Pu, K. Semiconducting Polymer Nanobioconjugates for Targeted Photothermal Activation of Neurons. *J. Am. Chem. Soc.* **138**, 9049–9052 (2016).
13. Winter J.O., Liu T.Y., K. B. A. and S. C. E. Recognition Molecule Directed Interfacing Between Semiconductor Quantum Dots and Nerve Cells. *Adv. Mater.* **13**, 1673–1677 (2001).
14. Lugo, K., Miao, X., Rieke, F. & Lin, L. Y. Remote switching of cellular activity and cell signaling using light in conjunction with quantum dots. *Biomed. Opt. Express* **3**, 447–54 (2012).
15. Pappas, T. C. *et al.* Nanoscale Engineering of a Cellular Interface with Semiconductor Nanoparticle Films for Photoelectric Stimulation of Neurons. *Nano Lett.* **7**, 513–519 (2007).
16. Bareket, L. *et al.* Semiconductor Nanorod – Carbon Nanotube Biomimetic Films for Wire-Free Photostimulation of Blind Retinas. *Nano Lett.* **14**, 6685–6692 (2014).
17. Schoen, I. & Fromherz, P. The mechanism of extracellular stimulation of nerve cells on an electrolyte-oxide-semiconductor capacitor. *Biophys. J.* **92**, 1096–1111 (2007).
18. Richter, C., Matic, A. I., Wells, J. D., Jansen, E. D. & Walsh, J. T. J. Neural stimulation with optical radiation. *Laser Photonics Rev.* **5**, 68–80 (2011).
19. Wells, J. *et al.* Biophysical mechanisms of transient optical stimulation of

- peripheral nerve. *Biophys. J.* **93**, 2567–80 (2007).
20. Migliori, B., Ventra, M. Di & Kristan, W. Photoactivation of neurons by laser-generated local heating. *AIP Adv.* **2**, 0–9 (2012).
 21. Pei, Z. M. *et al.* Calcium channels activated by hydrogen peroxide mediate abscisic acid signalling in guard cells. *Nature* **406**, 731–734 (2000).
 22. H. Richard Leuchtag. *Voltage-Sensitive Ion Channels Biophysics of Molecular Excitability. Book 1*, (Springer, 2008).
 23. Hamill, O. P., Marty, A., Neher, E., Sakmann, B. & Sigworth, F. J. Improved patch-clamp techniques for high-resolution current recording from cells and cell-free membrane patches. *Pflügers Arch. Eur. J. Physiol.* **391**, 85–100 (1981).
 24. Sakmann, B. and Neher, E. Patch Clamp Techniques for Studying Ionic Channels in Excitable Membranes. *Annu. Rev. Physiol.* **46**, 455–72 (1984).
 25. Lindau, M. & Fernandez, J. M. A patch-clamp study of histamine-secreting cells. *J. Gen. Physiol.* **88**, 349–368 (1986).
 26. Hill, M. *et al.* Characteristics of a Human Cell Line Transformed by D N A from Human Adenovirus Type 5. *J. Gen. Virol.* **36**, 59–74 (1977).
 27. Tang, W. Two-layer organic photovoltaic cell. *Appl. Phys. Lett.* **14650**, 1985–1987 (1986).
 28. Głowacki, E. D., Voss, G. & Sariciftci, N. S. 25th Anniversary Article : Progress in Chemistry and Applications of Functional Indigos for Organic Electronics. 1–18 (2013). doi:10.1002/adma.201302652
 29. Głowacki, E. D. *et al.* Hydrogen-Bonded Semiconducting Pigments for Air-Stable Field-Effect Transistors. *Adv. Mater.* **25**, 1563–1569 (2013).
 30. Głowacki, E. D. *et al.* Epindolidiones — Versatile and Stable Hydrogen-Bonded Pigments for Organic Field-Effect Transistors and Light-Emitting Diodes. *Adv. Funct. Mater.* **25**, 776–787 (2014).
 31. Głowacki, E. D. *et al.* Bioconjugation of hydrogen-bonded organic semiconductors with functional proteins. *J. Mater. Chem. C* **3**, 6554–6564 (2015).
 32. Sytnyk, M. *et al.* Hydrogen-Bonded Organic Semiconductor Micro- And Nanocrystals: From Colloidal Syntheses to (Opto-)Electronic Devices. (2014).
 33. Głowacki, E. D. *et al.* Indigo and Tyrian Purple - From Ancient Natural Dyes to Modern Organic Semiconductors. *Isr. J. Chem.* **52**, 540–551 (2012).
 34. Josephy, P. D., Eling, T. & Mason, R. P. The Horseradish Peroxidase-catalyzed Oxidation of 3,5,3',5'- Tetramethylbenzidine. *J. Biol. Chem.* **257**, 3669–3675 (1982).
 35. Ghezzi, D. *et al.* A polymer optoelectronic interface restores light sensitivity in blind rat retinas. *Nat. Photonics* **7**, 400–406 (2013).
 36. Brüggemann, D. *et al.* Nanostructured gold microelectrodes for extracellular recording from electrogenic cells. *Nanotechnology* **22**, 265104 (2011).
 37. Hofmann, B., Kätelhön, E., Schottdorf, M., Offenhäusser, A. & Wolfrum, B. Nanocavity electrode array for recording from electrogenic cells. *Lab Chip* **11**, 1054–1058 (2011).
 38. Santoro, F., Schnitker, J., Panaitov, G. & Offenhäusser, A. On chip guidance and recording of cardiomyocytes with 3D mushroom-shaped electrodes. *Nano Lett.* **13**, 5379–5384 (2013).
 39. Verma, P. & Melosh, N. A. Gigaohm resistance membrane seals with stealth probe electrodes. *Appl. Phys. Lett.* **97**, 8–11 (2010).

40. Cohen-Karni, T. & Lieber, C. M. Nanowire nanoelectronics: Building interfaces with tissue and cells at the natural scale of biology. *Pure Appl. Chem.* **85**, 883–901 (2013).
41. Chiappini, C. *et al.* Biodegradable Nanoneedles for Localized Delivery of Nanoparticles in Vivo : Exploring the Biointerface. *ACS Nano* **9**, 5500–5509 (2015).
42. Elnathan, R. *et al.* Maximizing Transfection Efficiency of Vertically Aligned Silicon Nanowire Arrays. *Adv. Funct. Mater.* **25**, 7215–7225 (2015).
43. Lu, Z. Mechanism of rectification in inward-rectifier K⁺ channels. *Annu. Rev. Physiol.* **66**, 103–129 (2004).
44. Hibino, H. *et al.* Inwardly Rectifying Potassium Channels: Their Structure, Function, and Physiological Roles. *Physiol. Rev.* **90**, 291–366 (2010).
45. D.L.Lewis, S.R.Ikeda, D.Aryee, R. H. J. Expression of an inwardly rectifying K⁺ channel from rat basophilic leukemia cell mRNA in *Xenopus* oocytes. *FEBS Lett.* **290**, 17–21 (1991).
46. Striessnig, J. *et al.* Role of voltage-gated L-type Ca²⁺ channel isoforms for brain function. *Biochem Soc Trans* **34**, 903–909 (2006).
47. Catterall, W. A. Voltage-Gated Calcium Channels. *Cold Spring Harb. Perspect. Biol.* **3**, (2011).
48. Kaltenbrunner, M. *et al.* Flexible high power-per-weight perovskite solar cells with chromium oxide–metal contacts for improved stability in air. *Nat. Mater.* **14**, 1032–1039 (2015).
49. Głowacki, E. D. *et al.* Hydrogen-Bonded Semiconducting Pigments for Air-Stable Field-Effect Transistors. *Adv. Mater.* **25**, 1563–1569 (2013).
50. Yao, J., Liu, B. & Qin, F. Rapid temperature jump by infrared diode laser irradiation for patch-clamp studies. *Biophys. J.* **96**, 3611–9 (2009).
51. Caterina, M. J. *et al.* The capsaicin receptor: a heat-activated ion channel in the pain pathway. *Nature* **389**, 816–824 (1997).
52. Szallasi, A., Cortright, D. N., Blum, C. a & Eid, S. R. The vanilloid receptor TRPV1: 10 years from channel cloning to antagonist proof-of-concept. *Nat. Rev. Drug Discov.* **6**, 357–372 (2007).
53. Albert, E. S. *et al.* TRPV4 channels mediate the infrared laser-evoked response in sensory neurons. *J. Neurophysiol.* **107**, 3227–3234 (2012).
54. Shapiro, M. G., Homma, K., Villarreal, S., Richter, C.-P. & Bezanilla, F. Infrared light excites cells by changing their electrical capacitance. *Nat. Commun.* **3**, 736 (2012).
55. Jakešová, M. *et al.* Hydrogen-Bonded Organic Semiconductors as Stable Photoelectrocatalysts for Efficient Hydrogen Peroxide Photosynthesis. *Adv. Funct. Mater.* **26**, 5248–5254 (2016).
56. Herson, P. S., Lee, K., Pinnock, R. D., Hughes, J. & Ashford, M. L. J. Hydrogen peroxide induces intracellular calcium overload by activation of a non-selective cation channel in an insulin-secreting cell line. *J. Biol. Chem.* **274**, 833–841 (1999).
57. Holzmann, C. *et al.* Differential Redox Regulation of Ca²⁺ Signaling and Viability in Normal and Malignant Prostate Cells. *Biophys. J.* **109**, 1410–1419 (2015).
58. Mathieson, K. *et al.* Photovoltaic retinal prosthesis with high pixel density. *Nat. Photonics* **6**, 391–397 (2012).

6. Curriculum Vitae

Name Marie Jakešová
Date of Birth September 14, 1991
Nationality Czech Republic
Email marie.jakesova@jku.at



EDUCATION

2014 – expected graduation January/February 2017

Double-degree master program Biological Chemistry

Johannes Kepler University (JKU), Linz, Austria

The University of South Bohemia (SBU), České Budějovice, Czech Republic

2011 – 2014

Double-degree bachelor program Biological Chemistry

Johannes Kepler University (JKU), Linz, Austria

The University of South Bohemia (SBU), České Budějovice, Czech Republic

RESEARCH EXPERIENCE

11/2016 – 12/2016 *Research assistant, JKU*

Institute of Biophysics, Ion Channels (R. Schindl)

Research assistant work on cell viability and interaction with organic semiconductors

08/2014 – 09/2016 *Research assistant and Master thesis project, JKU*

Linz Institute for Organic Solar Cells (LIOS) (N. S. Sariciftci)

Thesis: "Cellular photostimulation with hydrogen-bonded organic semiconductor microcrystal interfaces"

Research assistant work on photoelectrochemistry of organic semiconductors

01/2014 – 02/2014 *Bachelor thesis project, JKU*

Department of Organic Chemistry (N. Müller)

"Overexpression and purification of ¹³C, ¹⁵N labelled PsbP extrinsic protein of Photosystem II"

10/2012 – 08/2013 *Bachelor thesis project, SBU*

Laboratory of Developmental Biology and Genomics (A. W. Bruce)

"The role of Csf1 during preimplantation mouse development"

08/2009 – 1/2010 *Secondary school study project*

Department of Medical Genetics

Children's Medical Center (M. Hanáková)

"Cytogenetic Methods"

SCIENTIFIC CONTRIBUTIONS

Jakešová, M. Apaydin, D. H., Sytnyk, M., Oppelt, K., Heiss, W., Sariciftci, N. S. and Głowacki, E. D. Hydrogen-Bonded Organic Semiconductors as Stable Photoelectrocatalysts for Efficient Hydrogen Peroxide Photosynthesis. *Adv. Funct. Mater.* 26, 5248–5254 (2016).

Sytnyk, M., **Jakešová, M.**, Sariciftci, N. S., Heiss, W., and Głowacki, E. D. (2016). Cellular interfaces with biomimetic organic semiconductor hierarchical nanocrystals (under revision)

Poster prize, a 15 min oral presentation, for the Poster contribution at Asilomar Bioelectronics Symposium 2016, Monterey, CA, USA September 4–8, 2016 “Cellular photostimulation with hydrogen-bonded organic semiconductor microcrystal interfaces”

Contributed talk at ACS National Meeting, Philadelphia, PA, USA August 21-25, 2016 “Cellular photostimulation with hydrogen-bonded organic semiconductor microcrystal interfaces”

Poster presentation at International Symposium for the 80th Birthday of Prof. Alan J. Heeger, Linz, Austria March 21, 2016 “Stable photodriven hydrogen peroxide evolution using hydrogen-bonded organic semiconductors as photocathodes”

Poster presentation at BioEI 2016 International Winterschool on Bioelectronics, Kirchberg in Tirol, Austria, March 12–19, 2016 “Cellular photostimulation with hydrogen-bonded organic semiconductor microcrystal interfaces”

Poster presentation at BioEI 2015 International Winterschool on Bioelectronics, Kirchberg in Tirol, Austria, February 28 – March 7, 2015 “Biofunctionalization of hydrogen-bonded pigment semiconductors with Horseradish peroxidase”

TECHNICAL SKILLS

Biological techniques:

Mouse embryo collection and *in vitro* culture, immuno-staining, confocal microscopy imaging, polymerase chain reaction, dsRNA preparation, protein overexpression in *E. coli*, protein purification chromatography (affinity, ion exchange and size exclusion), ¹⁵N and ¹³C labelling for protein NMR, cell line culture *in vitro*, patch-clamp technique, preparation of biological specimen for scanning and transmission electron microscopy, spectrophotometric enzymatic assays

Materials science techniques:

Physical vapour deposition of organic films and metals, solution-processing of organic films, electrochemistry and photoelectrochemistry, organic thin film semiconductor devices and electrical characterization methods, scanning electron microscopy, optical microscopy techniques, profilometry, optical spectroscopy methods, colloidal synthesis

FURTHER EDUCATION

06/2010 Cambridge CAE certificate (English language, level C1)

01/2009 – 07/2009 Semester at Long Bay College, Auckland, New Zealand

OTHER WORK EXPERIENCE

07/2011 - present	Oltis Group, a.s. - English / Czech translations
10/2014 – 02/2015	JKU - Tutor for Organic Chemistry Laboratory
Summer 2011, 2012	Au-pair at Robert's family, Chiddingfold, England

LANGUAGES

Czech (native), English (proficiency), German (fluent), Spanish (fluent)